CORA Cork Open Research Archive
Cartlann Taighde Oscailte Chorcaí

Title	Exceptionally preserved fossil assemblages through geologic time and space
Authors	Muscente, A. D.;Schiffbauer, James D.;Broce, Jesse;Laflamme, Marc;O'Donnell, Kenneth;Boag, Thomas H.;Meyer, Michael;Hawkins, Andrew D.;Huntley, John Warren;McNamara, Maria E.;MacKenzie, Lindsay A.;Stanley Jr, George D.;Hinman, Nancy W.;Hofmann, Michael H.;Xiao, Shuhai
Publication date	2017-04-26
Original Citation	Muscente, A. D., Schiffbauer, J. D., Broce, J., Laflamme, M., O'Donnell, K., Boag, T. H., Meyer, M., Hawkins, A. D., Huntley, J. W., McNamara, M. E., MacKenzie, L. A., Stanley Jr, G. D., Hinman, N. W., Hofmann, M. H. and Xiao, S. (2017) 'Exceptionally preserved fossil assemblages through geologic time and space', Gondwana Research, 48, pp. 164-188. doi:10.1016/j.gr.2017.04.020
Type of publication	Article (peer-reviewed)
Link to publisher's version	10.1016/j.gr.2017.04.020
Rights	© 2017, International Association for Gondwana Research. Published by Elsevier B.V. All rights reserved. This manuscript version is made available under the CC-BY-NC-ND 4.0 license. - http://creativecommons.org/licenses/by-nc-nd/4.0/
Download date	2026-10-31 18:25:42
Item downloaded from	https://hdl.handle.net/10468/4593

UCC
University College Cork, Ireland
Coláiste na hOllscoile Corcaigh

Supplementary Information for

Exceptionally preserved fossil assemblages through geologic time and space

A. D. Muscente[a*], James D. Schiffbauer[b], Jesse Broce[b], Marc Laflamme[c], Kenneth O'Donnell[d], Thomas H. Boag[e], Michael Meyer[f], Andrew D. Hawkins[g], John Warren Huntley[b], Maria McNamara[h], Lindsay, A. MacKenzie[i], George D. Stanley Jr.[j], Nancy W. Hinman[j], Michael. H. Hofmann[j], and Shuhai Xiao[g]

[a]Department of Earth and Planetary Sciences, Harvard University, Cambridge, MA 02138, USA
[b]Department of Geological Sciences, University of Missouri, Columbia, MO 65211, USA
[c]Department of Chemical and Physical Sciences, University of Toronto Mississauga, Mississauga, ON L5L 1C6, Canada
[d]AECOM, Germantown, MD 20876, USA
[e]Department of Geological Sciences, Stanford University, Stanford, CA 94305, USA
[f]Geophysical Laboratory, Carnegie Institution for Science, Washington, DC 20015, USA
[g]Department of Geosciences, Virginia Tech, Blacksburg, VA 24061, USA
[h]School of Biological, Earth, and Environmental Sciences, University College Cork, Cork, T23 TK30, Ireland
[i]Department of Geological Sciences, SUNY Geneseo, Geneseo, NY 14454, USA
[j]Department of Geosciences, University of Montana, Missoula, MT 59812, USA

Corresponding author at: Department of Earth and Planetary Sciences, Harvard University, Cambridge, MA 02138, USA. Email address: a.d.muscente@gmail.com (A. D. Muscente).

Table of Contents

	Page
Supplementary Data (Dataset 1) caption | Data accompanying the paper	3
Animation S1 caption | Exceptional assemblages through geologic time and space	3
Animation S2 caption | Depositional settings of assemblages through geologic time	3

Supplementary figures		Page
Figure S1	Maps of geographic locations of exceptionally-preserved assemblages	4
Figure S2	Paleolatitude distributions of assemblages and PBDB fossil collections	5
Figure S3	Error of Euclidean distances used in hierarchical clustering	6
Figure S4	Cluster counts in 30.5 million year time bins for various methods	7
Figure S5	Cluster counts in 20.33 million year time bins for various methods	8
Figure S6	Cluster counts and proportions from clustering assemblages within chronostratigraphic intervals	9
Figure S7	First-difference testing of correlation results	10
Figure S8	Correlation and first-difference testing of assemblages clustered within chronostratigraphic intervals	11
Figure S9	Marine proportion results for various clustering methods	13
Figure S10	Transitional proportion results for various clustering methods	15
Figure S11	Non-marine proportion results for various clustering methods	17

Supplementary Methods, Discussion, and Equations		Page
1	Age, geographic location, and paleolatitude estimates	19
2	Paleoenvironmental and time binning	20
3	Sampling of Paleobiology Database (PBDB) collection data	20
4	Geographic binning analyses	21
5	Conversion of geographic coordinates to Cartesian coordinates	21
6	Geospatial statistics	22
7	Hierarchical clustering	23
8	Euclidean distance error	25
9	Overview of time series generated via hierarchical clustering in this study	26
10	Global sedimentary rock outcrop area estimates	30
11	Global sedimentary rock volume estimates	32
12	North American surface/subsurface rock area estimates	33
13	Description of trends in rock quantities through geologic time	33
14	Statistical testing of cluster counts and proportions	33
15	First-difference testing	35
16	Results of clustering assemblages within chronostratigraphic intervals	35
17	References for supplementary information	39

Table of Contents (cont.)

Supplementary tables		Page
Table S1	Overview of time series produced via clustering assemblages of the global dataset (i.e. the entire database) in equal duration time bins	27
Table S2	Overview of time series produced via clustering assemblages of the North American subset of database in equal duration time bins	28
Table S3	Overview of time series produced via clustering assemblages of the global dataset (i.e. the entire database) in chronostratigraphic intervals	29
Table S4	List of chronostratigraphic intervals used in hierarchical clustering	38

Supplementary Data (Dataset S1). Excel file containing dataset of exceptionally preserved fossil assemblages as well as other data and results accompanying the paper.

Animation S1. Plate motion model showing distribution of exceptionally-preserved fossil assemblages through geologic time and space. This animation shows the exceptionally preserved assemblages in each geologic system at their paleogeographic locations (yellow indicators) and at their times of preservation (measured in "Mega anna," Ma). Blue lines indicate approximate boundaries of tectonic plates.

Animation S2. Plate motion model showing depositional settings of exceptionally-preserved fossil assemblages through geologic time. This animation shows the exceptionally preserved assemblages of each depositional setting category at their paleogeographic locations and at their times of preservation (Ma). Gray lines indicate approximate boundaries of tectonic plates; blue, red, and green indicators denote exceptionally preserved fossil assemblages from marine, transitional, and non-marine depositional settings, respectively.

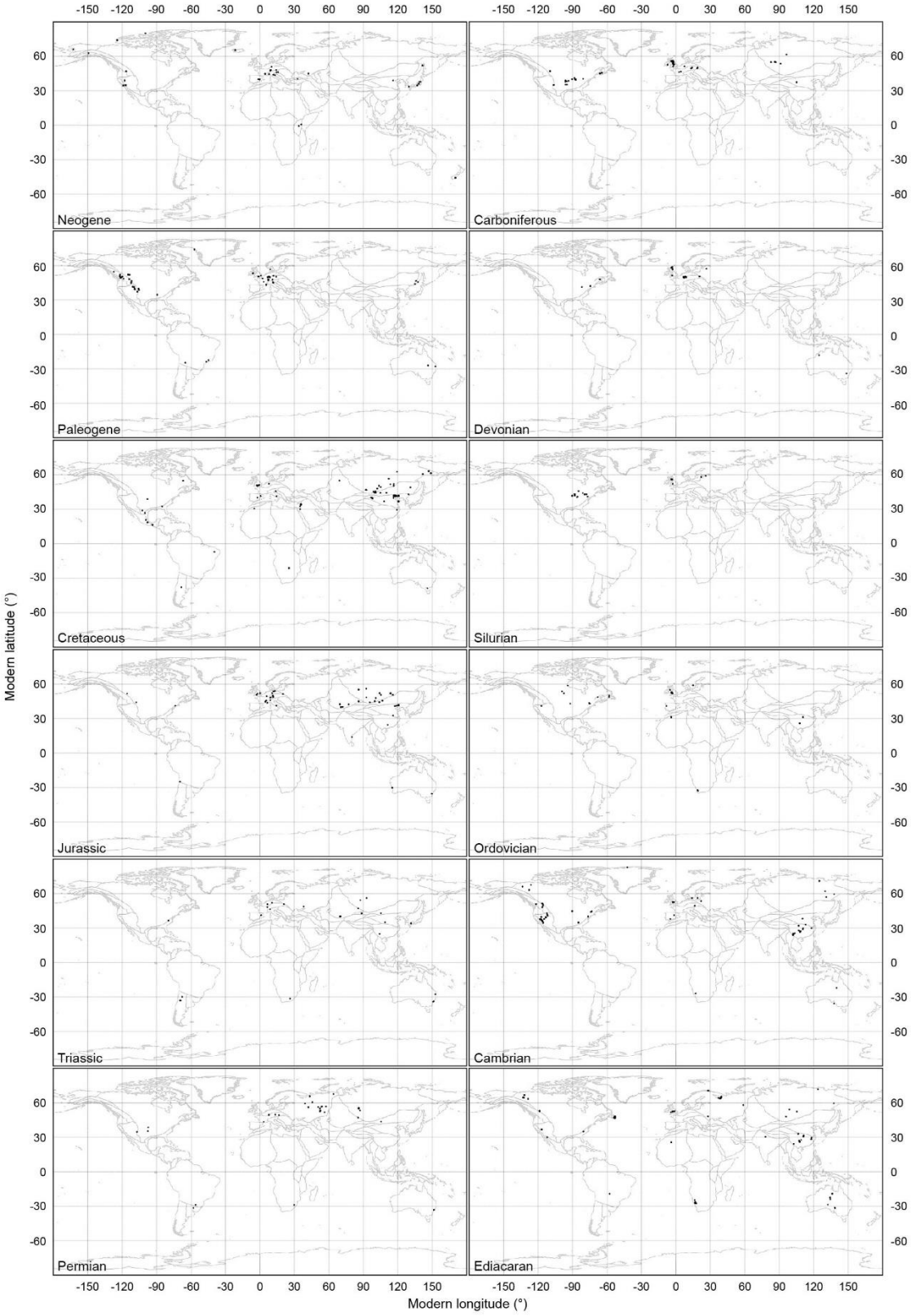

Fig. S1. Maps of geographic locations of exceptionally-preserved assemblages in each system.

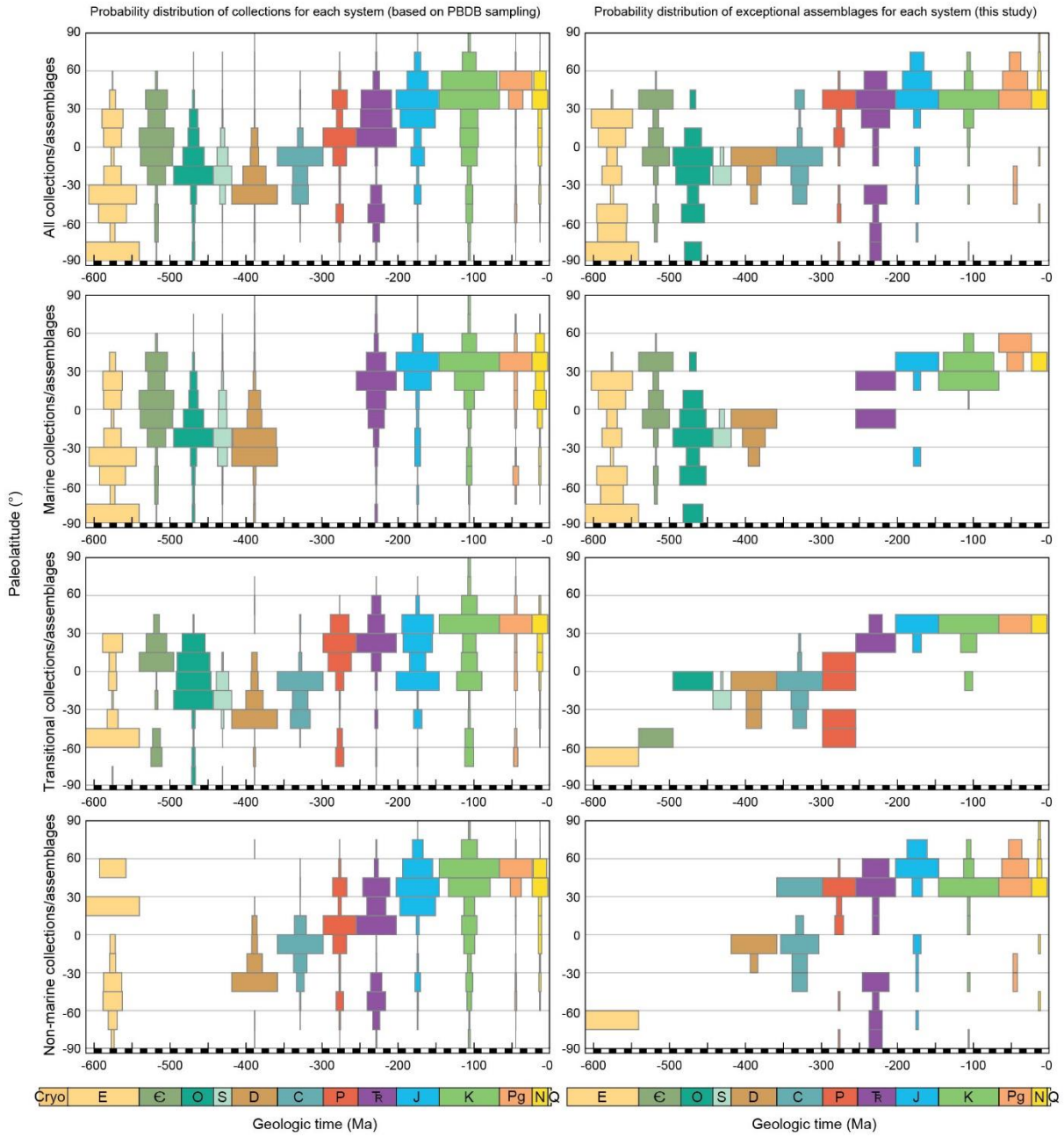

Fig. S2. Paleolatitude distributions of exceptionally preserved assemblages and randomly sampled PBDB fossil collections for Ediacaran-Neogene geologic systems. Rows correspond to different depositional setting categories included in the distributions; the left column includes distributions of PBDB collections; and the right column includes distributions of exceptionally-preserved assemblages. Cryo, Cryogenian; E, Ediacaran; Є, Cambrian; O, Ordovician; S, Silurian; D, Devonian; C, Carboniferous; P, Permian, Tr, Triassic; J, Jurassic; K, Cretaceous; Pg, Paleogene; N, Neogene; Q, Quaternary.

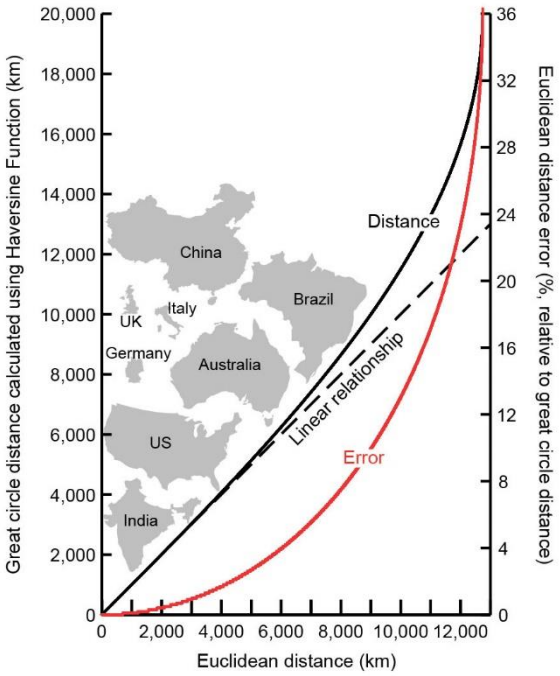

Fig. S3. Error of Euclidean distances used in hierarchical clustering. Solid black line shows relationship between Euclidean and great circle distance calculations; dashed line shows linear relationship; and red line shows percentage error in Euclidean (relative to great circle) distance. Countries included at Euclidean distance scale for reference.

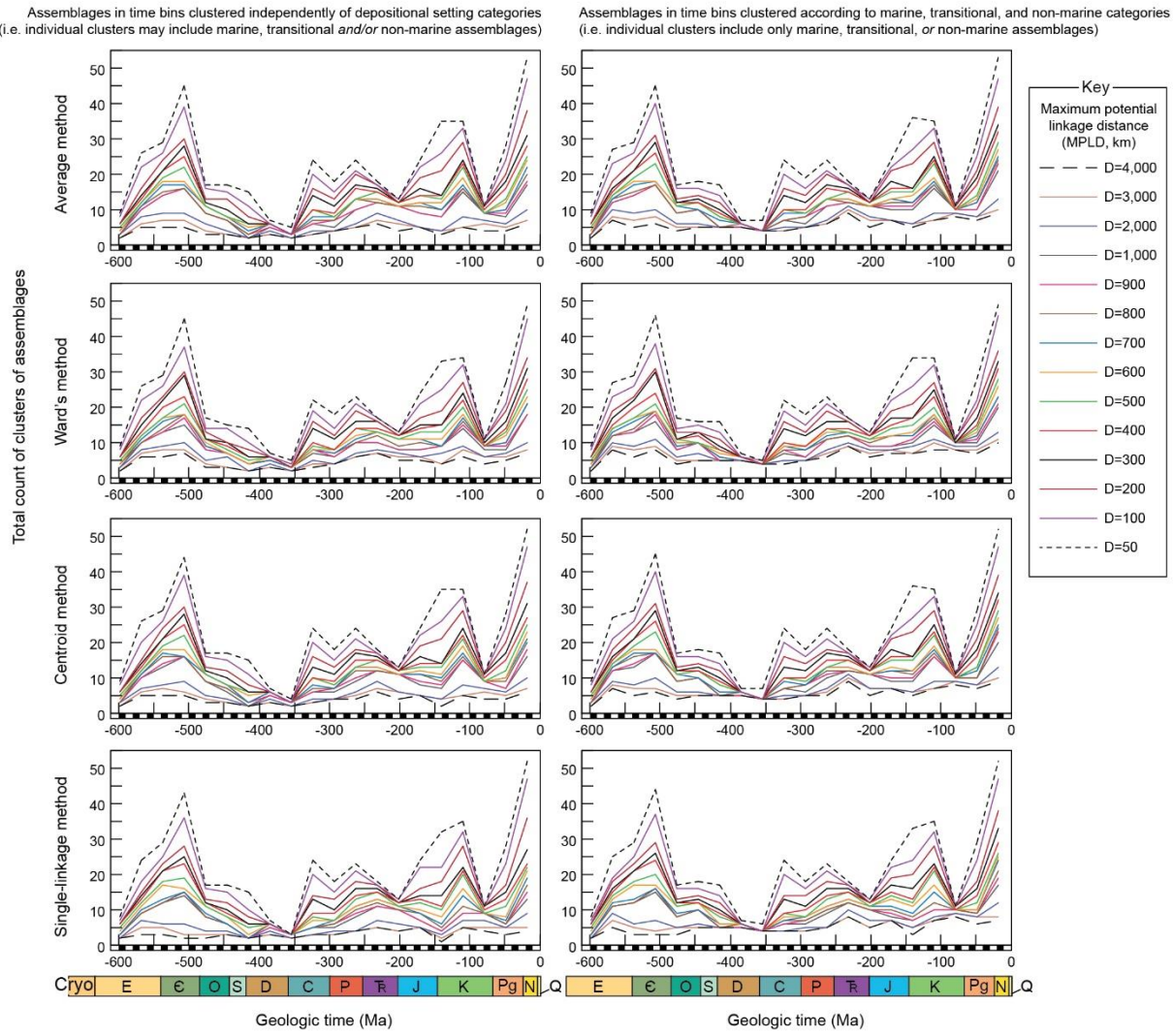

Fig. S4. Cluster counts in 30.5 million year duration time bins. For all plots, the *x* axis is geologic time and *y* axis is the number of clusters. Assemblages in left and right columns were hierarchically clustered independently of and according to marine, transitional, and non-marine depositional setting categories, respectively. Rows correspond to different clustering methods. Note that the results are generally similar regardless of the clustering method (rows) and data categories (columns) used in cluster counting. Cryo, Cryogenian; E, Ediacaran; Є, Cambrian; O, Ordovician; S, Silurian; D, Devonian; C, Carboniferous; P, Permian, Tr, Triassic; J, Jurassic; K, Cretaceous; Pg, Paleogene; N, Neogene; Q, Quaternary.

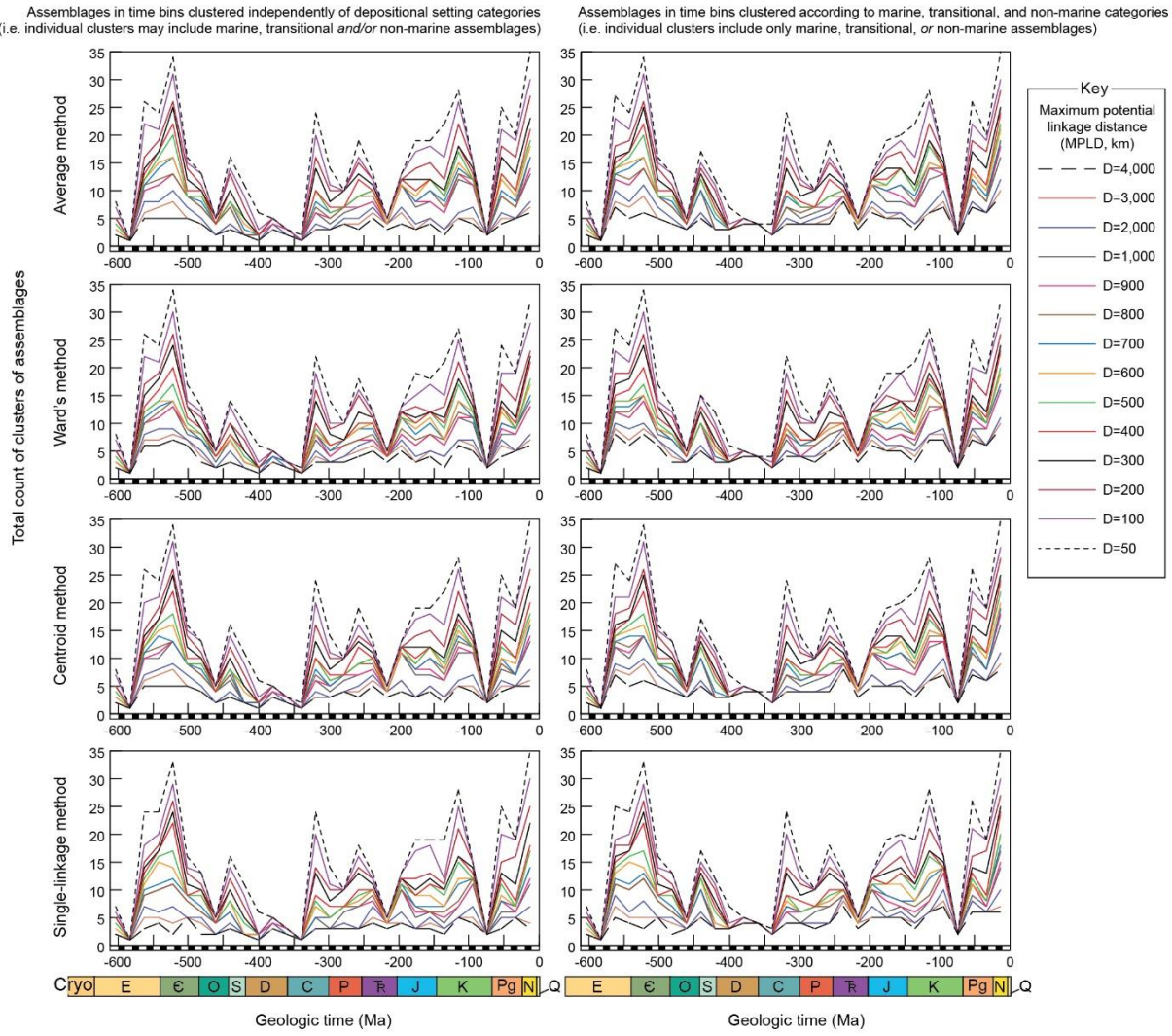

Fig. S5. Cluster counts in 20.3 million year duration time bins. For all plots, the *x* axis is geologic time and *y* axis is the number of clusters. Assemblages in left and right columns were hierarchically clustered independently of and according to marine, transitional, and non-marine depositional setting categories, respectively. Rows correspond to different clustering methods. Note that the results are generally similar regardless of the clustering method (rows) and data categories (columns) used in cluster counting. Cryo, Cryogenian; E, Ediacaran; Є, Cambrian; O, Ordovician; S, Silurian; D, Devonian; C, Carboniferous; P, Permian, Tr, Triassic; J, Jurassic; K, Cretaceous; Pg, Paleogene; N, Neogene; Q, Quaternary.

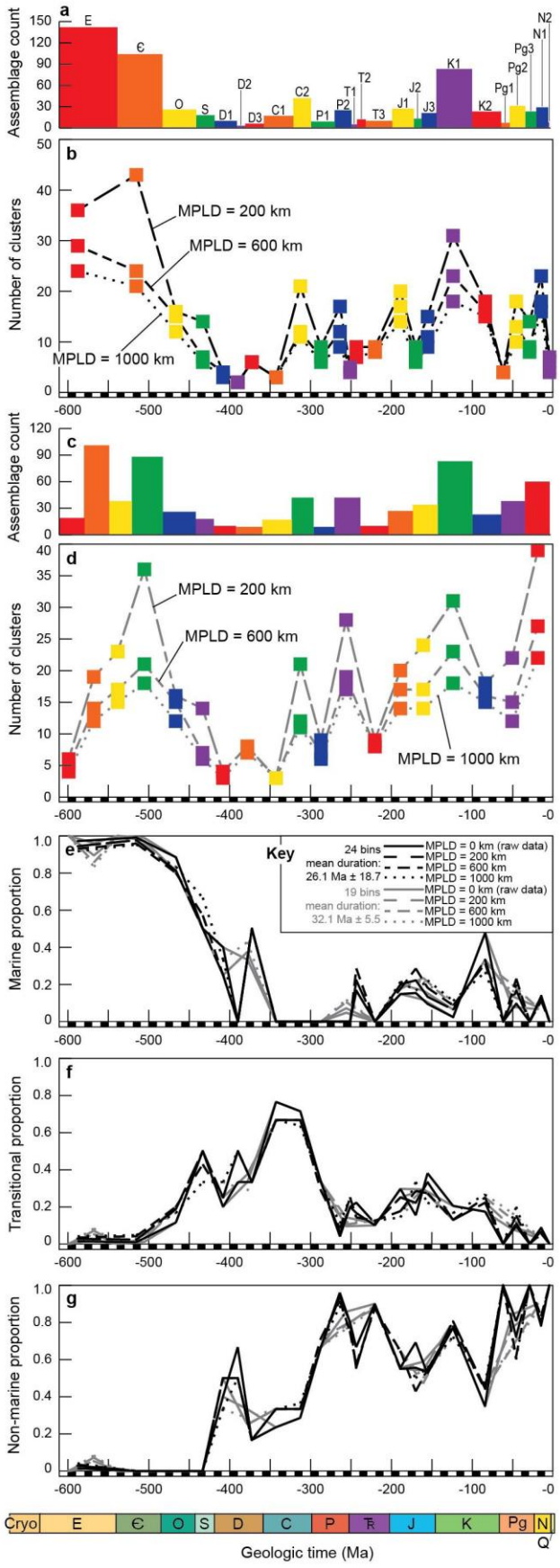

Fig. S6. Cluster counts and proportions from hierarchical clustering of assemblages within chronostratigraphic intervals listed in Table S4. (a–d) Assemblage and cluster counts. Cluster counts represent totals of marine, non-marine, and transitional clusters. (a, b) Assemblages clustered within 24 chronostratigraphic intervals (mean duration 26.1 Ma ± 18.7). These intervals are equivalent to systems and series (see Table S4 for abbreviations), except for P2, which corresponds to the Guadalupian and Lopingian (this unit was selected to match available rock quantity data). (a) Bar chart showing raw assemblage count in each system or series. (b) Plot showing total (marine+transitional+non-marine) cluster count for each system or series for three representative MPLDs: 200 km, 600 km, and 1000 km. (c, d) Assemblages clustered within 19 chronostratigraphic intervals (mean duration 32.1 Ma ± 5.5), representing systems, series, and combinations of series and/or Ediacara-type fossil biozones. These intervals represent relatively less varied geologic times than those in (a, b). (c) Bar chart showing raw assemblage count in each interval. (b) Plot showing total (marine+transitional+non-marine) cluster count for each interval for three representative MPLDs: 200 km, 600 km, and 1000 km. (e–g) Plots showing proportions versus geologic time for the data in (a–d), as indicated in key in (e). (e) Proportion of marine clusters. (f) Proportion of transitional clusters. (g) Proportion of non-marine clusters. Note that results are consistent with analyses based on equal duration time bin data (Figs. 7, 12, 14, S9-S11).

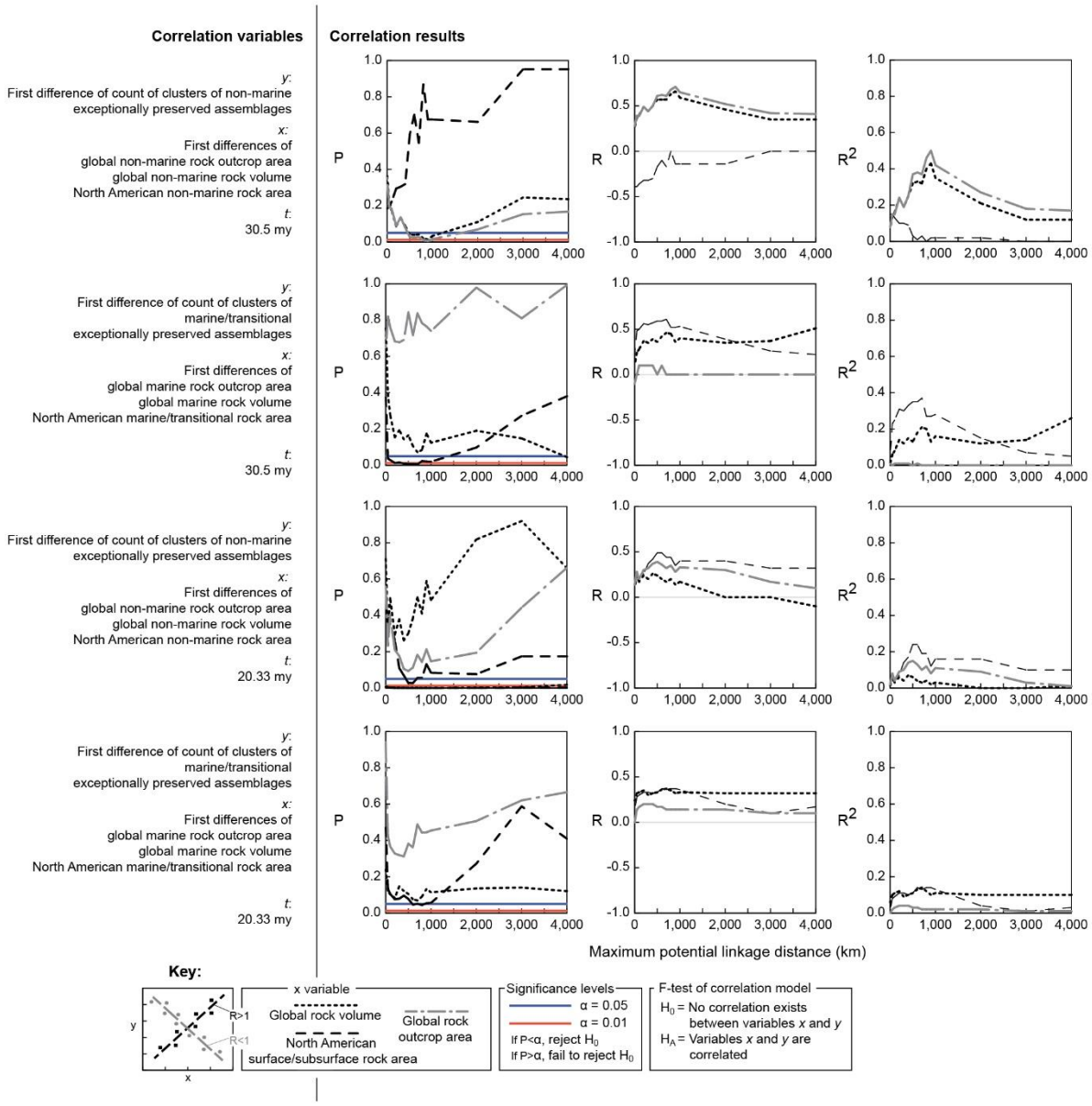

Fig. S7. First-difference testing of correlations. First differences of cluster counts (clusters identified within equal duration time bins), global rock outcrop areas, global rock volumes, and North American surface/subsurface rock areas were compared. First differences of cluster counts based on various maximum potential linkage distances (MPLDs) were determined for 30.5 million year (my) and 20.33 my duration (t) time bins using the complete-linkage method. For all plots, x-axis is MPLD. The *y* axes in the left, middle, and right columns correspond to P, R, and R^2 values, respectively, for the correlations of the x and y first differences listed on the left. Lines in the plots correspond to specific x variable first differences, indicated in the key. Whereas the first differences of cluster counts compared to first differences of global rock outcrop areas and global rock volumes are based on the entire database of exceptionally preserved assemblages, the first differences of cluster counts compared to first differences of North American rock areas are based only on the North American subset of the database.

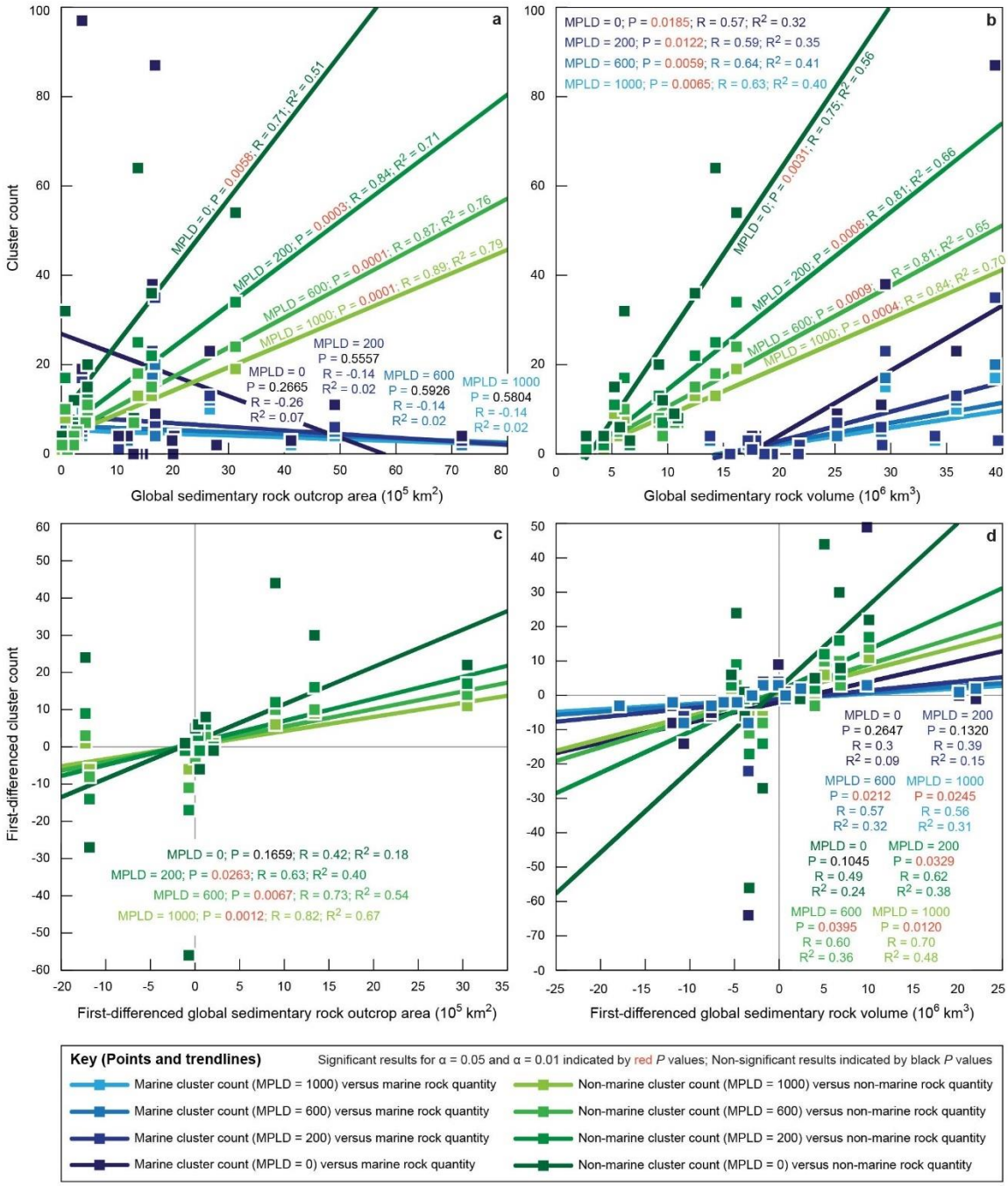
a
Cluster count
Global sedimentary rock outcrop area (10^5 km^2)
MPLD = 0; P = 0.0058; R = 0.71; R^2 = 0.51
MPLD = 200; P = 0.0003; R = 0.84; R^2 = 0.71
MPLD = 600; P = 0.0001; R = 0.87; R^2 = 0.76
MPLD = 1000; P = 0.0001; R = 0.89; R^2 = 0.79
MPLD = 200 P = 0.5557 R = -0.14 R^2 = 0.02
MPLD = 0 P = 0.2665 R = -0.26 R^2 = 0.07
MPLD = 600 P = 0.5926 R = -0.14 R^2 = 0.02
MPLD = 1000 P = 0.5804 R = -0.14 R^2 = 0.02
b
MPLD = 0; P = 0.0185; R = 0.57; R^2 = 0.32
MPLD = 200; P = 0.0122; R = 0.59; R^2 = 0.35
MPLD = 600; P = 0.0059; R = 0.64; R^2 = 0.41
MPLD = 1000; P = 0.0065; R = 0.63; R^2 = 0.40
MPLD = 0; P = 0.0031; R = 0.75; R^2 = 0.56
MPLD = 200; P = 0.0008; R = 0.81; R^2 = 0.66
MPLD = 600; P = 0.0009; R = 0.81; R^2 = 0.65
MPLD = 1000; P = 0.0004; R = 0.84; R^2 = 0.70
Global sedimentary rock volume (10^6 km^3)
c
First-differenced cluster count
First-differenced global sedimentary rock outcrop area (10^5 km^2)
MPLD = 0; P = 0.1659; R = 0.42; R^2 = 0.18
MPLD = 200; P = 0.0263; R = 0.63; R^2 = 0.40
MPLD = 600; P = 0.0067; R = 0.73; R^2 = 0.54
MPLD = 1000; P = 0.0012; R = 0.82; R^2 = 0.67
d
MPLD = 0 P = 0.2647 R = 0.3 R^2 = 0.09
MPLD = 200 P = 0.1320 R = 0.39 R^2 = 0.15
MPLD = 600 P = 0.0212 R = 0.57 R^2 = 0.32
MPLD = 1000 P = 0.0245 R = 0.56 R^2 = 0.31
MPLD = 0 P = 0.1045 R = 0.49 R^2 = 0.24
MPLD = 200 P = 0.0329 R = 0.62 R^2 = 0.38
MPLD = 600 P = 0.0395 R = 0.60 R^2 = 0.36
MPLD = 1000 P = 0.0120 R = 0.70 R^2 = 0.48
First-differenced global sedimentary rock volume (10^6 km^3)
Key (Points and trendlines)
Significant results for α = 0.05 and α = 0.01 indicated by red P values; Non-significant results indicated by black P values
Marine cluster count (MPLD = 1000) versus marine rock quantity
Marine cluster count (MPLD = 600) versus marine rock quantity
Marine cluster count (MPLD = 200) versus marine rock quantity
Marine cluster count (MPLD = 0) versus marine rock quantity
Non-marine cluster count (MPLD = 1000) versus non-marine rock quantity
Non-marine cluster count (MPLD = 600) versus non-marine rock quantity
Non-marine cluster count (MPLD = 200) versus non-marine rock quantity
Non-marine cluster count (MPLD = 0) versus non-marine rock quantity

Fig. S8. Correlation and first-difference testing analyses of cluster counts derived by hierarchical clustering assemblages within 19 chronostratigraphic intervals (mean duration 32.1 Ma ± 5.5) representing systems, series, and combinations of series and Ediacara-type fossil biozones (Table S4). (a, b) Marine and non-marine counts (y-axis), based on various MPLDs, are compared with global sedimentary rock outcrop area and volume (x-axes). Whereas analyses involving marine counts and outcrop area include all bins (n=19), those involving marine counts and volumes exclude the oldest two bins (n=17), as no data is available on global Ediacaran rock volume. Analyses involving non-marine counts exclude bins older than the early Devonian (n=13), as animals did not colonize terrestrial environments until the late Silurian. Correlations between marine cluster count and rock volume excluded time bins older than 551 Ma, as rock volume data is not available for the Ediacaran. (a) Counts versus outcrop area. (b) Count versus rock volume. (c, d) First-difference testing results for statistical significant correlations in (a, b). In these plots, first-differenced cluster count (y-axis) is compared with first-differenced outcrop area and rock volume (x-axes). The numbers of bins in these analyses are n-1, compared to the values in (a, b). (c) First-differenced cluster count versus first-differenced rock outcrop area. (d) First-differenced cluster count versus first-differenced rock volume. For all analyses, data points and trendlines are plotted, and significant results are indicated by *P* values in red.

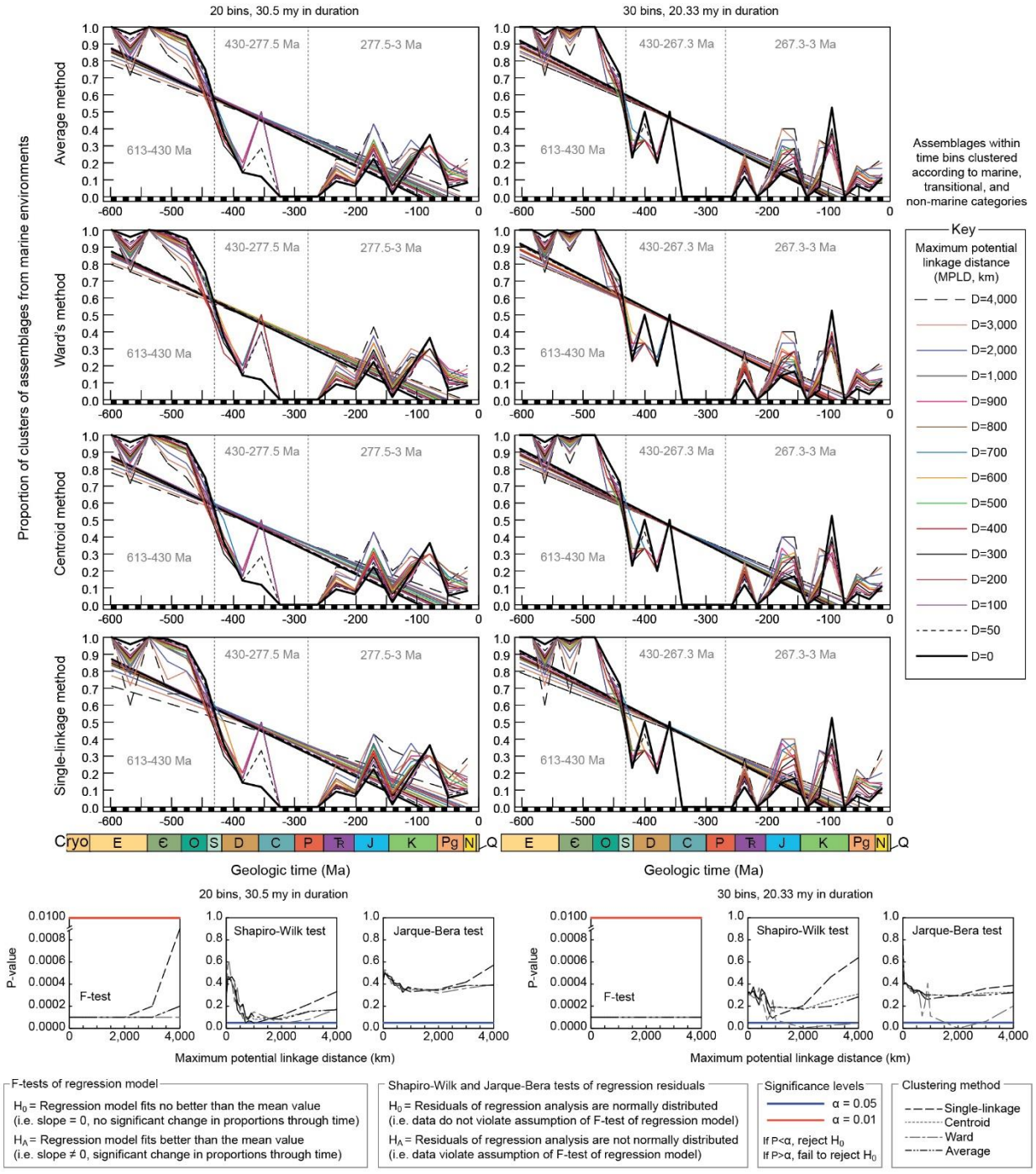
20 bins, 30.5 my in duration
30 bins, 20.33 my in duration
Average method
Ward's method
Centroid method
Single-linkage method
Proportion of clusters of assemblages from marine environments
430-277.5 Ma
277.5-3 Ma
613-430 Ma
430-267.3 Ma
267.3-3 Ma
Assemblages within time bins clustered according to marine, transitional, and non-marine categories
Key
Maximum potential linkage distance (MPLD, km)
D=4,000
D=3,000
D=2,000
D=1,000
D=900
D=800
D=700
D=600
D=500
D=400
D=300
D=200
D=100
D=50
D=0
Cryo E Є O S D C P Ŧ J K Pg N Q
Geologic time (Ma)
P-value
F-test
Shapiro-Wilk test
Jarque-Bera test
Maximum potential linkage distance (km)
F-tests of regression model
H0 = Regression model fits no better than the mean value (i.e. slope = 0, no significant change in proportions through time)
HA = Regression model fits better than the mean value (i.e. slope ≠ 0, significant change in proportions through time)
Shapiro-Wilk and Jarque-Bera tests of regression residuals
H0 = Residuals of regression analysis are normally distributed (i.e. data do not violate assumption of F-test of regression model)
HA = Residuals of regression analysis are not normally distributed (i.e. data violate assumption of F-test of regression model)
Significance levels
α = 0.05
α = 0.01
If P<α, reject H0
If P>α, fail to reject H0
Clustering method
Single-linkage
Centroid
Ward
Average

Fig. S9. Marine proportions. Assemblages clustered according to marine, transitional, and non-marine depositional setting categories within equal duration time bins. For all rectangular plots, the *x* axis is geologic time and *y* axis is the proportion of clusters; columns correspond to different time bin durations; rows correspond to different clustering methods; and vertical lines delineate time domains. Linear 1st-degree polynomial regression models fit to the time series are also included in the rectangular plots. For all square plots, the *x* axis is maximum potential linkage distance and *y* axis is P value. P values were compiled from F, Shapiro-Wilk, and Jarque-Bera testing. Note that the results are generally similar regardless of clustering method (rows) and time bin duration (columns). Cryo, Cryogenian; E, Ediacaran; Є, Cambrian; O, Ordovician; S, Silurian; D, Devonian; C, Carboniferous; P, Permian, Tr, Triassic; J, Jurassic; K, Cretaceous; Pg, Paleogene; N, Neogene. Q, Quaternary.

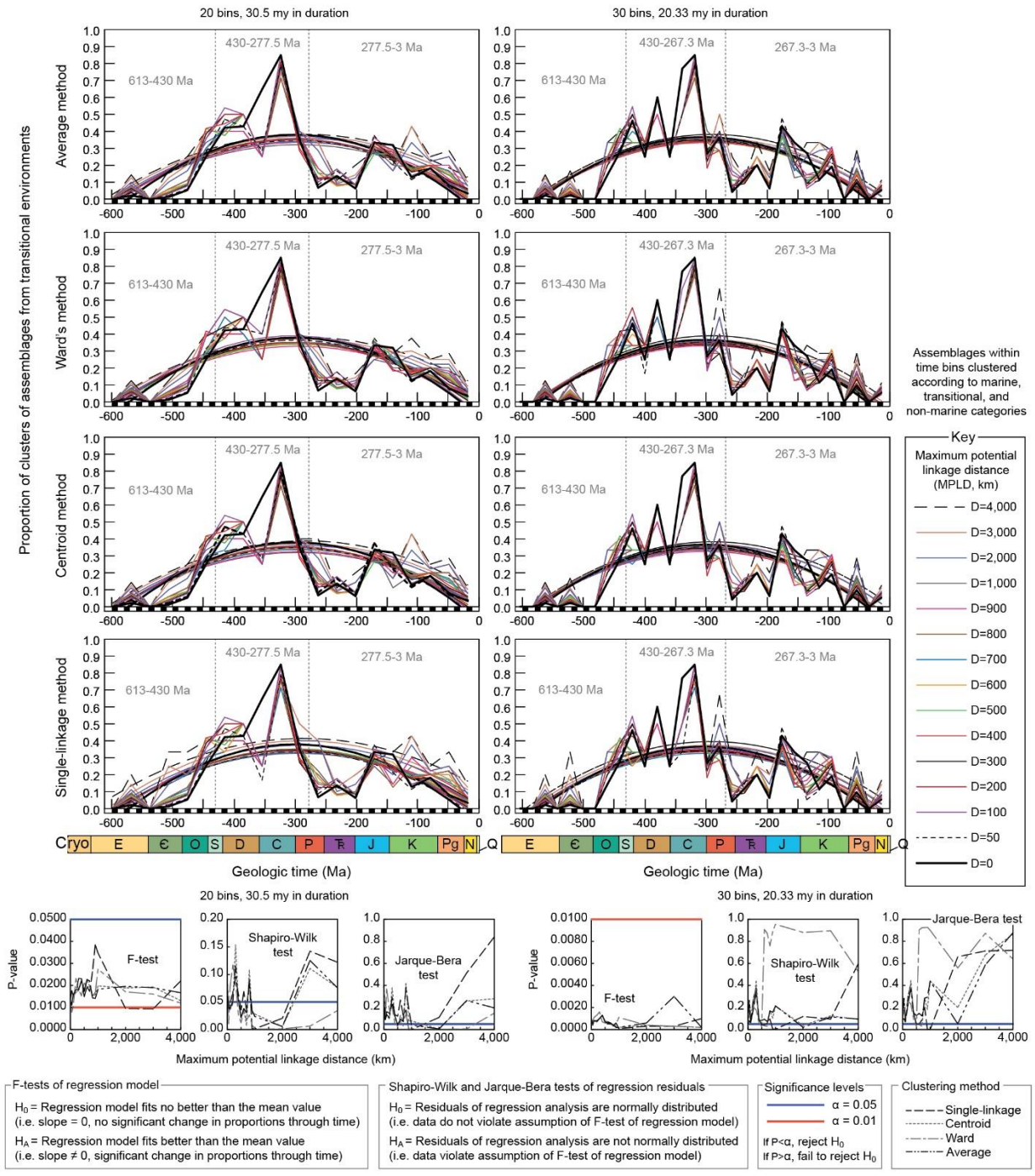
20 bins, 30.5 my in duration
30 bins, 20.33 my in duration
Proportion of clusters of assemblages from transitional environments
Average method
Ward's method
Centroid method
Single-linkage method
613-430 Ma
430-277.5 Ma
277.5-3 Ma
430-267.3 Ma
267.3-3 Ma
Cryo E Є O S D C P Ŧ J K Pg N Q
Geologic time (Ma)
Assemblages within time bins clustered according to marine, transitional, and non-marine categories
Key
Maximum potential linkage distance (MPLD, km)
D=4,000
D=3,000
D=2,000
D=1,000
D=900
D=800
D=700
D=600
D=500
D=400
D=300
D=200
D=100
D=50
D=0
P-value
F-test
Shapiro-Wilk test
Jarque-Bera test
Maximum potential linkage distance (km)
F-tests of regression model
H0 = Regression model fits no better than the mean value (i.e. slope = 0, no significant change in proportions through time)
HA = Regression model fits better than the mean value (i.e. slope ≠ 0, significant change in proportions through time)
Shapiro-Wilk and Jarque-Bera tests of regression residuals
H0 = Residuals of regression analysis are normally distributed (i.e. data do not violate assumption of F-test of regression model)
HA = Residuals of regression analysis are not normally distributed (i.e. data violate assumption of F-test of regression model)
Significance levels
α = 0.05
α = 0.01
If P<α, reject H0
If P>α, fail to reject H0
Clustering method
Single-linkage
Centroid
Ward
Average

Fig. S10. Transitional proportions. Assemblages clustered according to marine, transitional, and non-marine depositional setting categories within equal duration time bins. For all rectangular plots, the *x* axis is geologic time and *y* axis is the proportion of clusters; columns correspond to different time bin durations; rows correspond to different clustering methods; and vertical lines delineate time domains. Linear 2nd-degree polynomial regression models fit to the time series are also included in the rectangular plots. For all square plots, the *x* axis is maximum potential linkage distance and *y* axis is P value. P values were compiled from F, Shapiro-Wilk, and Jarque-Bera testing. Note that the results are generally similar regardless of clustering method (rows) and time bin duration (columns). Cryo, Cryogenian; E, Ediacaran; Є, Cambrian; O, Ordovician; S, Silurian; D, Devonian; C, Carboniferous; P, Permian, Tr, Triassic; J, Jurassic; K, Cretaceous; Pg, Paleogene; N, Neogene. Q, Quaternary.

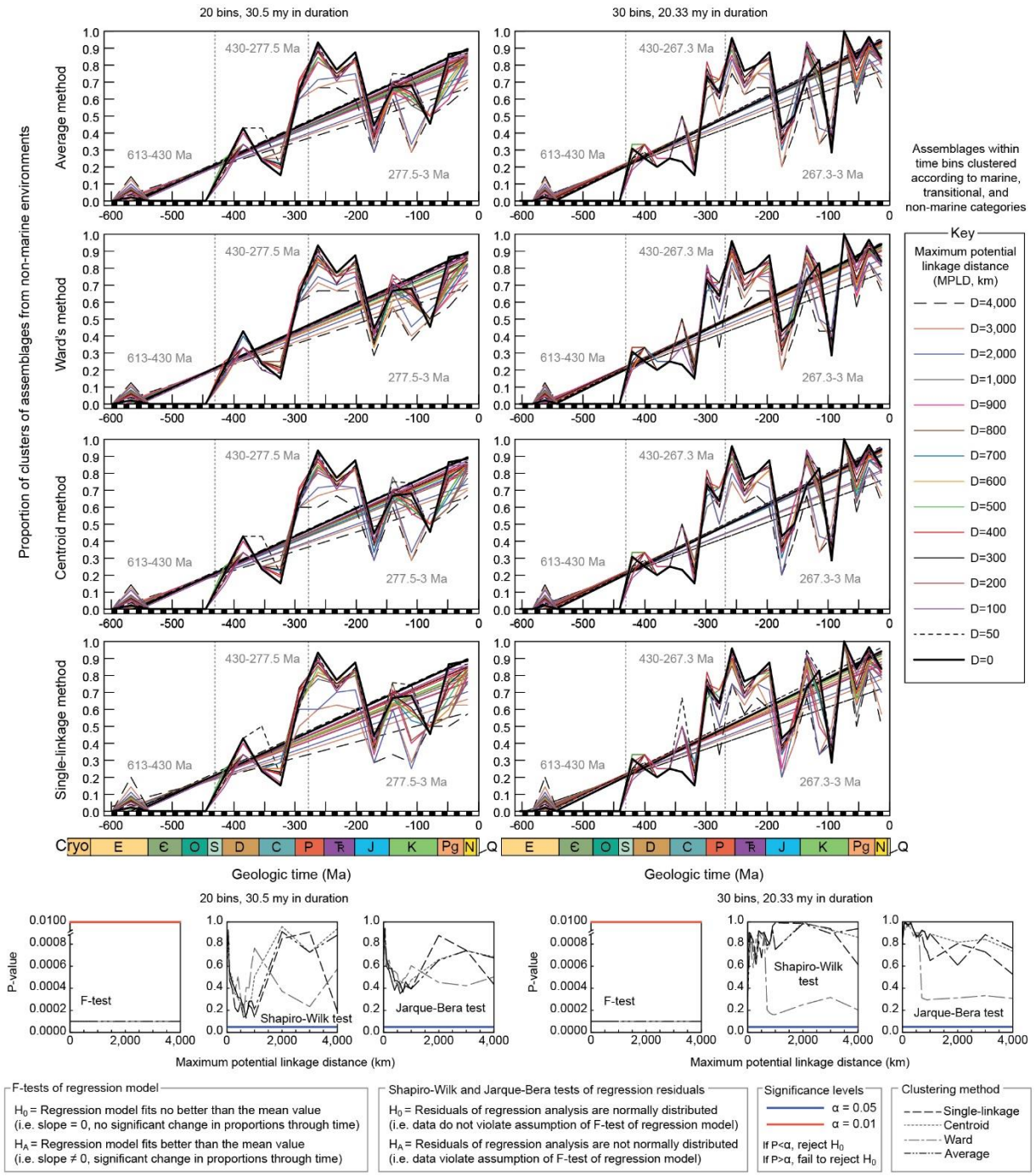
20 bins, 30.5 my in duration
30 bins, 20.33 my in duration
Average method
Ward's method
Centroid method
Single-linkage method
Proportion of clusters of assemblages from non-marine environments
430-277.5 Ma
613-430 Ma
277.5-3 Ma
430-267.3 Ma
267.3-3 Ma
Assemblages within time bins clustered according to marine, transitional, and non-marine categories
Key
Maximum potential linkage distance (MPLD, km)
D=4,000
D=3,000
D=2,000
D=1,000
D=900
D=800
D=700
D=600
D=500
D=400
D=300
D=200
D=100
D=50
D=0
Cryo E Є O S D C P Ŧ J K Pg N Q
Geologic time (Ma)
P-value
F-test
Shapiro-Wilk test
Jarque-Bera test
Maximum potential linkage distance (km)
F-tests of regression model
H0 = Regression model fits no better than the mean value (i.e. slope = 0, no significant change in proportions through time)
HA = Regression model fits better than the mean value (i.e. slope ≠ 0, significant change in proportions through time)
Shapiro-Wilk and Jarque-Bera tests of regression residuals
H0 = Residuals of regression analysis are normally distributed (i.e. data do not violate assumption of F-test of regression model)
HA = Residuals of regression analysis are not normally distributed (i.e. data violate assumption of F-test of regression model)
Significance levels
α = 0.05
α = 0.01
If P<α, reject H0
If P>α, fail to reject H0
Clustering method
Single-linkage
Centroid
Ward
Average

Fig. S11. Non-marine proportions. Assemblages clustered according to marine, transitional, and non-marine depositional setting categories within equal duration time bins. For all rectangular plots, the *x* axis is geologic time and *y* axis is the proportion of clusters; columns correspond to different time bin durations; rows correspond to different clustering methods; and vertical lines delineate time domains. Linear 1st-degree polynomial regression models fit to the time series are also included in the rectangular plots. For all square plots, the *x* axis is maximum potential linkage distance and *y* axis is P value. P values were compiled from F, Shapiro-Wilk, and Jarque-Bera testing. Note that the results are generally similar regardless of clustering method (rows) and time bin duration (columns). Cryo, Cryogenian; E, Ediacaran; Є, Cambrian; O, Ordovician; S, Silurian; D, Devonian; C, Carboniferous; P, Permian, Tr, Triassic; J, Jurassic; K, Cretaceous; Pg, Paleogene; N, Neogene. Q, Quaternary.

1. Age, geographic location, and paleolatitude estimates

Estimated ages of Phanerozoic assemblages are the means of the absolute upper and lower ages of their chronostratigraphic units, as specified in the International Chronostratigraphic Chart (ICC; Cohen et al., 2013). For assemblages in the Ediacaran, for which series and stages have not yet been established, estimated ages are means of absolute ages from radiometrically dated beds stratigraphically bracketing the assemblages. The ages of Ediacaran assemblages in sequences without radiometrically dated beds were estimated based on their stratigraphic positions relative to putative Ediacara-type macrofossil biozones (Narbonne et al., 2012) and Neoproterozoic glaciations (Hoffman and Li, 2009) with absolute age constraints in other sections. In any case, most assemblages are constrained to ages in Earth history, and all but two are resolved to epochs. The average uncertainty in the ages of the assemblages is 5 Ma with a standard deviation of 5 Ma.

Latitudinal and longitudinal coordinates were estimated from maps based on nearby landmarks. Paleolatitudes of assemblages were estimated, based on their ages and modern geographic positions (Fig. S1), using the global plate motion model (file: Phanerozoic_EarthByte.rot) produced by Wright et al. (2013) in *GPlates* (Qin et al., 2012; Williams et al., 2012; Fig. 4d; Animations S1, S2). The model is a reconstruction of plate motion from 580 Ma to the present. All assemblages were entered in the *GPlates* program as point features at their current geographic positions (time: 0 Ma), and individually saved as *.gmpl* files (allowing for future analyses in *GPlates* with other plate motion models). These *.gmpl* files were then loaded into the program with the Wright et al. (2013) model and the standard coastline features file (Phanerozoic_EarthByte_Coastlines.gpml; Qin et al., 2012; Williams et al., 2012; Wright et al., 2013). For assemblages younger than 580 (n=675), paleolatitude estimates were derived from the reconstructed latitudinal coordinates of their point features at the times corresponding to their ages. Paleolatitude estimates for assemblages older than 580 (n=19) were taken from the reconstructed latitudinal coordinates of their point features at 580 Ma. The exact ages of pre-580 Ma assemblages—which include the Zuun-Arts biota (Dornbos et al., 2016), the Taoudenni Basin Ediacara-type fossils (Bertrand-Sarfati et al., 1995), and various assemblages in the Doushantuo (Muscente et al., 2015) and equivalent Lantian (Yuan et al., 2011) formations of South China—are controversial (Bertrand-Sarfati et al., 1995; Muscente et al., 2015). Thus, multiple uncertainties confound estimation of their paleolatitudes. Nonetheless, because the pre-580 Ma assemblages represent relatively small fractions of the overall dataset (<3%, 19/694) and Ediacaran subset (<14%, 19/142), the uncertainties regarding their paleolatitudes likely did not strongly influence the results of the analyses.

To assess the accuracy of the paleolatitude estimates from *GPlates* relative to those derived using other approaches, we compiled supplementary estimates of paleolatitude (Fig. 4e) for 548 of the assemblages from collection entries in the Paleobiology Database (PBDB). Some assemblages in this study correspond to multiple collections in the PBDB. In these cases, the most common paleolatitude value among the PBDB collections was selected as the supplementary estimate. If the collections were evenly split among two values, the mean value was calculated and recorded as the estimate. Many of the assemblages of exceptionally preserved fossils in this study did not have fossil collections listed in Fossilworks, and their paleolatitudes could not always be acquired from the PBDB. Even so, for some of these assemblages,

paleolatitudes were estimated based on collections of non-exceptional fossils (i.e. biomineralized skeletal elements) from the same geologic units (e.g. formation or member) as the exceptional fossils. Overall, the estimates from *GPlates* (Fig. 4d) and the estimates from the PBDB (Fig. 4e) are similar (mean absolute difference±standard deviation, 9.5 degrees ± 11.6), particularly for the post-Cambrian assemblages (mean absolute difference±standard deviation, 5.0 degrees ± 5.0). We therefore conclude that the *GPlates* estimates are reasonably accurate.

2. Paleoenvironmental and time binning

Assemblages were assigned—based on descriptions of their paleoenvironments in the literature—to mutually exclusive marine, transitional, and non-marine depositional setting categories, as well as an indeterminate category for assemblages that are not well constrained. The marine category includes assemblages from subtidal inner continental shelf, inner continental shelf basin, outer continental shelf, continental slope, and basin (continental rise and abyssal plain) paleoenvironments. The transitional category includes those from estuaries, deltas, lagoons (restricted bodies of water separated from the open ocean by barriers), bays (restricted bodies of water encompassed on most of their sides by shoreline), supratidal zones, sabhkas, and tidal (sand and mud) flats. Finally, the non-marine category includes those from lakes and rivers. Assemblages from marine and transitional environments were additionally assigned to a combined marine/transitional category.

Based on their ages, assemblages were assigned to time bins comprising two time series: a time series of 30.5 (n=20) million year (my) equal duration time bins and another of 20.3 (n=30) my equal duration time bins. We selected these durations because their corresponding time series identically span the shortest geochronological interval (3–613 Ma) that encompasses all assemblages in the dataset albeit with different numbers of time bins (n=20 for 30.5 my; n=30 for 20.3 my). Based on their time bins, assemblages were additionally assigned to time domains, which were compared via statistical difference testing (see supplementary section 14). The assemblages in the 30.5 my time bins were assigned to 613–430 Ma (Ediacaran–early Paleozoic), 430–277.5 Ma (middle–late Paleozoic), 277.5–3 Ma (Mesozoic–Cenozoic), 277.5–186 Ma (early Mesozoic), 186–64 Ma (late Mesozoic), and 64–3 Ma (Cenozoic) domains; and those in the 20.3 my time bins were assigned to 613–430 Ma (Ediacaran–early Paleozoic), 430–267.3 Ma (middle–late Paleozoic), 267.3–3 Ma (Mesozoic–Cenozoic), 267.3–186 Ma (early Mesozoic), 186–145.3 Ma (Jurassic), 145.3–104.7 Ma (early Cretaceous), 104.7–84.3 Ma (middle Cretaceous), and 84.3–3 Ma (late Cretaceous-Cenozoic) domains.

3. Sampling of PBDB collection data

A comprehensive snapshot of collections was compiled from the PBDB on December 11, 2015. Each fossil collection in the PBDB was assigned to one of the four previously defined depositional setting categories—marine, transitional, non-marine, or indeterminate—based on its paleoenvironment (Dataset S1 includes a comprehensive list of classes in the "environment" field in the PBDB and their corresponding depositional setting categories). Then, 500 samples (each with 694 collections, exactly matching the number of assemblages in our dataset) were randomly drawn with replacement from the list. For each sample, the count of collections from each geologic system (Ediacaran-Neogene) and depositional setting category (marine,

transitional, and non-marine environments) was controlled so that the distribution of collections among these systems and categories identically matches that of exceptionally preserved assemblages in the database (i.e. since seven exceptionally preserved marine assemblages occur in the Devonian, each sample includes exactly seven marine collections of Devonian age). Following this procedure, changes in the environmental preponderances and frequencies of exceptionally preserved assemblages through geologic time did not affect the analyses.

4. Geographic binning analyses

Assemblages and collections were assigned—based on their geographic locations and estimated ages and paleolatitudes—to latitudinal (n=12), longitudinal (n=24), and age/paleolatitudinal (n=144) bins. Latitudinal and longitudinal bins each correspond to 15 degrees of geographic range (e.g. 0–15°, 15–30°, etc.), and the 144 age/paleolatitudinal bins include 12 groups—corresponding to the 12 geologic systems—that consist of 12 bins, each representing 15 degrees of paleolatitude range. The counts of assemblages and the mean counts of PBDB collections among the 500 samples were determined for each bin. Lastly, for each bin type, the mean counts of collections were compared to the corresponding counts of exceptionally preserved assemblages through correlation analysis. The results are presented as *F*-test *P*, R, and R^2 values. Overall, in this approach, the count of exceptionally preserved assemblages is expected to be positively correlated (R>0) with the mean count of PBDB collections if the assemblages and collections have broadly similar geographic distributions. Significant ($P < 0.05$) and highly significant ($P < 0.01$) *F*-test *P* values with R values > 0, assuming $\alpha = 0.05$, are considered evidence that the distributions of the two datasets are broadly similar.

The results of the geographic binning analyses indicate that exceptionally preserved fossil assemblages and (principally skeletal) PBDB fossil collections generally have similar latitudinal, longitudinal, and age/paleolatitudinal distributions (Figs. 5, S2). Most sampled fossils occur in the northern hemisphere at latitudes between 30 and 60 degrees, and analyses of the latitudinal bins indicate a strong positive correlation (F-test P: 0.001; R: 0.930; R^2: 0.860) between the assemblage and collection counts in the bins. Likewise, the assemblages and collections follow similar tri-modal longitudinal distributions—with peaks in the -120 to -75 degree, -15 to 30 degree, and 105 to 120 degree ranges—that broadly correspond to the longitudinal ranges associated with maximum landmass (i.e. North and South America; Europe and Africa; and eastern Asia and Australia). Their counts in the longitudinal bins are also positively correlated (F-test P: 0.001; R: 0.830; R^2: 0.680). Lastly, correlation analyses (F-test P: 0.001; R: 0.760; R^2: 0.580) indicate that the occurrences of the assemblages and collection are broadly congruent in terms of age and paleolatitude. Therefore, no broad scale differences exist among the geographic distributions of exceptionally preserved and skeletal fossils.

5. Conversion of geographic coordinates to Cartesian coordinates

x is an observation (assemblage)
x_i is the ith observation (assemblage)
r is the radius of Earth
φ_i is the latitude geographic coordinate of x_i

λ_i is the longitude geographic coordinate of x_i

a_i is Cartesian coordinate 1 of x (measure along axis perpendicular to plane of the 90th east and 90th west meridians; longitudes >-90° or <90° have positive values and longitudes <-90° or >90° have negative values after conversion)

b_i is Cartesian coordinate 2 of x (measured along axis perpendicular to equatorial plane; latitudes >0° have positive values and latitudes <0° have negative values after conversion)

c_i is Cartesian coordinate 3 of x (measured along axis perpendicular to the International Greenwich prime meridional/antimeridional plane; longitudes <0° have negative values and longitudes >0° have positive values after conversion)

$$a_i = r \times \cos\left(\frac{\varphi_i \pi}{180}\right) \times \cos\left(\frac{\lambda_i \pi}{180}\right) \quad \text{(Eq. S1)}$$

$$b_i = r \times \sin\left(\frac{\varphi_x \pi}{180}\right) \quad \text{(Eq. S2)}$$

$$c_i = r \times \cos\left(\frac{\varphi_i \pi}{180}\right) \times \sin\left(\frac{\lambda_i \pi}{180}\right) \quad \text{(Eq. S3)}$$

6. Geospatial statistics

Nearest neighbor and geospatial statistical analyses were performed using the PASSaGE Windows version 2.0 software package (Rosenberg and Anderson, 2011). Ripley's K(d) and L(d)—functions for detecting deviations from geospatial homogeneity—were calculated for various subsets of the dataset in order to assess whether the assemblages are uniform, random, or clumped in their geographic distribution. The K(d) function represents a measure of the mean number of points (e.g. assemblages) found within a specific distance of each point, divided by the average density of points. For approximately two-dimensional datasets, such as the data in this study, distance corresponds to the radius of a circle around each point. For data analysis, we focused on Ripley's L(d), which is equal to distance minus K(d). Ignoring sample size effects, L(d) is generally equal to zero for randomly distributed points, greater than zero for uniformly spaced points; and less than zero for clumped points.

Overall, we calculated three types of L(d) values, each based on different combinations of points: (1) all assemblages regardless of their depositional settings (i.e. the entire dataset); (2) assemblages from matching depositional settings (i.e. the marine, transitional, or non-marine subsets); and (3) assemblages of different settings than the central point (e.g. marine and non-marine points counted around transitional assemblages; non-marine and transitional points counted around marine assemblages; and marine and transitional points counted around non-marine assemblages). These different types of values accordingly provide details about corresponding patterns of data homogeneity. In calculating these values, we assumed a two-dimensional study plot; used a 50 km step size and the latitudinal/longitudinal coordinates and great-circle distances of the assemblages; and controlled for study plot edge effects by applying

weights to the point counts. The weight of each point is inversely related to the area-based proportion of the circle around each point located within the plot area.

We performed two randomization tests to produce confidence intervals (CIs) for assessing the K(d) and L(d) values: (1) a geospatial homogeneity test and (2) a categorical association test. The first test involved the generation of a new point pattern in the study plot containing the same number of original points but with randomized locations. Overall, this procedure was repeated 99 times, and the 2.5 and 97.5 percentiles values of K(d) and L(d) among the replicates were determined. If the observed values fell within the 95% CI envelope, the values could be explained as sampling artefacts. Conversely, observed values occurring above and below the envelope represent significant evidence of assemblage regularity and clustering, respectively. For the second test, the locations of the assemblages remain constant, but their categories (i.e. depositional settings) were randomized with the number of each type held constant. As before, this procedure was repeated 99 times, and the 2.5 and 97.5 percentiles values of K(d) and L(d) among the replicates were determined. In this case, the randomization tests whether points occur randomly, regularly, or clumped in their distribution with respect to depositional setting.

Moran's I provides a measure of spatial autocorrelation (i.e. correlation in signal among proximally-located points). In this work, Moran's I and its critical values were calculated to assess spatial autocorrelation in geologic age amongst nearest neighbor pairs and amongst points located at various relative distances between 0 and 2000 km. For the latter work, we examined changes in Moran's I across distances classes (i.e. 0-50 km, 50-100 km, etc.). As with traditional correlation coefficient (R) calculations, values greater than 1 and less than 1 signify positive and negative correlation, respectively. To assess the significance of these values, we determined Z values and their corresponding probabilities.

7. Hierarchical clustering

The hierarchical clustering analyses in this study employed five methods of clustering. In all these methods—except for Ward's method, which is based on analysis of variance (ANOVA)—pairwise Euclidean distances represent the numerical metrics used in determining assemblage clustering order. The clustering methods, however, differ in their criteria for clustering (i.e. which observations are used to calculate the pairwise Euclidean distances and combine assemblages). A short overview of the equations used in these methods is provided below. For these equations, lowercase and uppercase symbols designate observations (assemblages) and clusters of observations (clusters of assemblages), respectively.

n is the number of observations (depends upon time bin and categories used in clustering)
v is the number of variables (equal to three for all hierarchical clustering analyses)
x_i is the ith observation (assemblage)
x_j is the jth observation (assemblage)
a_i, b_i, and c_i are the variables (Cartesian coordinates) of x_i
a_j, b_j, and c_j are the variables (Cartesian coordinates) of x_j
C_K is the K^{th} cluster (subset of 1, 2, 3 … n)
C_L is the L^{th} cluster (subset of 1, 2, 3 … n)

x is the sample mean vector
x_K is the mean vector for cluster C_K
x_L is the mean vector for cluster C_L
N_K is the number of observation in C_K
N_L is the number of observation in C_L
D_{KL} is the distance between the K^{th} and L^{th} clusters
$d(x_i, x_j)$ is the Euclidean distance between x_i and x_j:

Euclidean distance between assemblages

$$d(x_i, x_j) = \sqrt{(a_i - a_j)^2 + (b_i - b_j)^2 + (c_i - c_j)^2} \quad \text{(Eq. S4)}$$

Complete-linkage method

$$D_{KL} = \max_{i \in C_K \; j \in C_L} d(x_i, x_j) \quad \text{(Eq. S5)}$$

The distance between two clusters is the maximum distance between an observation in one cluster and an observation in the other cluster. This method tends to produce clusters of equal diameters (Milligan, 1980; Milligan and Cooper, 1987; Murtagh and Contreras, 2012).

Average method

$$D_{KL} = \sum_{i \in C_K} \sum_{j \in C_L} \frac{d(x_i, x_j)}{N_K \times N_L} \quad \text{(Eq. S6)}$$

The distance between two clusters is the average distance among pairs of observations (one from each cluster). This method favors the joining of clusters with small variances, and tends to produce clusters of equal variances (Milligan, 1980; Milligan and Cooper, 1987; Murtagh and Contreras, 2012; Sokal and Milchener, 1958).

Ward's minimum variance method

$$D_{KL} = \frac{\sqrt{(x_K + x_L)^2}}{\frac{1}{N_K} + \frac{1}{N_L}} \quad \text{(Eq. S7)}$$

The distance between two clusters is the ANOVA sum of squares between the two clusters, added up over all variables. At each step, clusters are joined that result in the minimum increase in total within-cluster variance weighted against square distance between cluster centers. This method tends to combine and produce clusters with approximately equal numbers of observations, and is sometimes sensitive to outliers (Milligan, 1980; Milligan and Cooper, 1987; Murtagh and Contreras, 2012).

Centroid method

(Eq. S8)

$$D_{KL} = \sqrt{(x_K + x_L)^2}$$

The distance between two clusters is equal to the squared Euclidean distance between their means. Results based on this method are generally robust to outliers (Milligan, 1980; Milligan and Cooper, 1987; Murtagh and Contreras, 2012).

Single-linkage method

(Eq. S9)

$$D_{KL} = \min_{i \in C_K \; j \in C_L} \mathrm{d}(x_i, x_j)$$

The distance between two clusters is the minimum distance an observation in one cluster and an observation in the other cluster (Milligan, 1980; Milligan and Cooper, 1987; Murtagh and Contreras, 2012). Depending on the observations, this method may produce elongated and irregularly-shaped clusters (i.e. long, thin clusters, in which adjacent observations are separated by relatively short distances, but observations on opposite ends of the cluster are separated by relatively great distances; Hartigan, 1981).

8. Euclidean distance error

The Euclidean distances used in hierarchical clustering signify 'straight line' distances rather than orthodromic distances. In order to investigate potential errors in Euclidean distances, the errors of Euclidean distances versus actual great-circle distances were calculated and compared for 32,672 unique pairs of geographic points on the Earth surface. With the exception of one—in which the geographic points had identical latitudes and longitudes (0, 0) and was included to provide an error-free baseline for the analysis—all the pairs were generated through random combining of points in a dataset of 65342 unique points. The geographic points in this dataset include all possible combinations of latitude (-90 to 90) and longitude (-180 to 180 longitude) integer coordinates. Following the procedures described above, the geographic points were converted to Cartesian coordinates (assuming the Earth is a perfect sphere with a radius of 6,371 km; Eqs. 1–3), and the Euclidean (Eq. S4) and great-circle distances between the points in each pair as well as the Euclidean distance errors (Eq. S10) were calculated (Fig. S3).

(Eq. S10)

$$\frac{|Euclidean\ distance - great\ circle\ distance|}{great\ circle\ distance} \times 100\ \% = Euclidean\ distance\ error$$

The great-circle distance (d) separating the geographic points in each pair was estimated using the Haversine Formula (*h*, Eq. 11), which is based on the Haversine function (Eq. 12).

x is an observation (assemblage)
x_i is the ith observation (assemblage)
x_j is the jth observation (assemblage)
r is the radius of Earth
φ_i is the latitude geographic coordinate of x_i

λ_i is the longitude geographic coordinate of x_i
φ_j is the latitude geographic coordinate of x_j
λ_j is the longitude geographic coordinate of x_j

(Eq. S11)

$$h = \text{hav}\left(\frac{d}{r}\right) = \text{hav}(\varphi_j - \varphi_i) + \cos(\varphi_i)\cos(\varphi_j)\,\text{hav}(\lambda_j - \lambda_i)$$

(Eq. S12)

$$\text{hav}(\theta) = \sin^2\left(\frac{\theta}{2}\right) = \frac{1 - \cos(\theta)}{2}$$

Based on these equations, d is calculated by applying the inverse haversine function (hav^{-1}) or arcsine function (Eqs. S13–S15).

(Eq. S13)

$$d = r \times \text{hav}^{-1}(h) = 2 \times r \times \arcsin(\sqrt{h})$$

(Eq. S14)

$$d = 2 \times r \times \arcsin\left(\sqrt{\text{hav}(\varphi_j - \varphi_i) + \cos(\varphi_i)\cos(\varphi_j)\,\text{hav}(\lambda_j - \lambda_i)}\right)$$

(Eq. S15)

$$d = 2 \times r \times \arcsin\left(\sqrt{\sin^2\left(\frac{\varphi_j - \varphi_i}{2}\right) + \cos(\varphi_i)\cos(\varphi_j)\sin^2\left(\frac{\lambda_j - \lambda_i}{2}\right)}\right)$$

Dataset S1 and Fig. S3 include the results of the Euclidean distance error analysis, showing a <1.7% error for the Euclidean distances (≤4000 km) used to identify clusters in this study. To ground truth the great-circle distances estimated using the Haversine Formula, the ground length distances separating the geographic distances in some pairs were assessed using the ruler tool in Google Earth. Some Haversine Formula estimates deviate from Google Earth ground length measurements because the Haversine Formula calculations do not account for Earth's ellipticity (varying radius and radius of curvature). Nonetheless, the error in the Haversine Formula estimates is generally low for geographic points separated by short (<4000 km) distances and occurring at nearly equal latitudes. Based on these findings, we conclude that the errors associated with the Euclidean distances used in identifying clusters in this study are generally minor, and did not significantly bias the results or conclusions of the analyses.

9. Overview of time series generated via hierarchical clustering in this study

Hierarchical clustering based on various time bin durations/chronostratigraphic intervals, clustering methods, MPLDs, data fractions (global dataset versus North American subset), and data categories (fractions of dataset used in clustering, e.g. marine/transitional vs. non-marine)

resulted in compilation of cluster counts and proportions (Dataset S1). These cluster counts and proportions, in turn, comprise assorted time series (Tables S1–S3). These time series were analyzed in time bin cluster count equality testing (i.e. Pearson's chi-square equality and randomization testing), time domain homogeneity testing (i.e. Pearson's chi-square homogeneity and Fisher's exact testing), and linear polynomial regression model fitting, which incorporated F-, Shapiro-Wilk, and Jarque-Bera testing (see supplementary section 14). The results of these tests are presented as cross-plots of test statistic (P) value and MPLD.

Table S1. Overview of the global cluster count/proportion time series generated by hierarchical clustering within equal duration time bins in this study. Each time series corresponds to a unique time bin duration, data category (or combination of data categories), clustering method, and maximum potential linkage distance (MPLD) combination. All time series in this table are based on the global dataset (i.e. the entire database).

Time Bin Duration	Fraction of global dataset used in clustering	No. clustering methods	No. MPLDs	Total no. time series
30.5	All (clustered within time bins independently of depositional setting category)*	5	15	75
30.5	Marine assemblages	5	15	75
30.5	Non-marine assemblages	5	15	75
30.5	Transitional assemblages	5	15	75
30.5	All (clustered within time bins according to depositional setting categories)†	5	15	75
30.5	Marine/transitional assemblages	1	15	15
30.5	All (clustered within time bins according to depositional setting categories)‡	1	15	15
20.33	All (clustered within time bins independently of depositional setting category)*	5	15	75
20.33	Marine assemblages	5	15	75
20.33	Non-marine assemblages	5	15	75
20.33	Transitional assemblages	5	15	75
20.33	All (clustered within time bins according to depositional setting categories)†	5	15	75
20.33	Marine/transitional assemblages	1	15	15
20.33	All (clustered within time bins according to depositional setting categories)‡	1	15	15
			Total:	**810**

*clusters in counts may include marine, transitional, and/or non-marine assemblages

† cluster counts equal sums of corresponding marine, transitional, and non-marine counts

‡ cluster counts equal sums of corresponding marine/transitional and non-marine counts

Table S2. Overview of the North American cluster count time series generated via hierarchical clustering in this study. Each time series corresponds to a unique time bin duration, data category (or combination of data categories), clustering method, and maximum potential linkage distance (MPLD) combination. All time series in this table are based on hierarchical clustering of the assemblages in the North American subset of the database within time bins according the complete-linkage method.

Time Bin Duration	Fraction of North American dataset used in clustering	No. clustering methods	No. MPLDs	No. time series
30.5	All (clustered within time bins independently of depositional setting category)*	1	15	15
30.5	Marine assemblages	1	15	15
30.5	Non-marine assemblages	1	15	15
30.5	Transitional assemblages	1	15	15
30.5	All (clustered within time bins according to depositional setting categories)†	1	15	15
30.5	Marine/transitional assemblages	1	15	15
30.5	All (clustered within time bins according to depositional setting categories)‡	1	15	15
20.33	All (clustered within time bins independently of depositional setting category)*	1	15	15
20.33	Marine assemblages	1	15	15
20.33	Non-marine assemblages	1	15	15
20.33	Transitional assemblages	1	15	15
20.33	All (clustered within time bins according to depositional setting categories)†	1	15	15
20.33	Marine/transitional assemblages	1	15	15
20.33	All (clustered within time bins according to depositional setting categories)‡	1	15	15
			Total:	**210**

*clusters in counts may include marine, transitional, and/or non-marine assemblages

† cluster counts equal sums of corresponding marine, transitional, and non-marine counts

‡ cluster counts equal sums of corresponding marine/transitional and non-marine counts

Table S3. Overview of the global cluster count/proportion time series generated by hierarchical clustering within chronostratigraphic intervals (Table S4) in this study. Each time series corresponds to a unique chronostratigraphic interval set, data category (or combination of data categories), clustering method, and maximum potential linkage distance (MPLD) combination. All time series in this table are based on hierarchical clustering of the assemblages in the global dataset (i.e. the entire database) according the complete-linkage method.

Set of Intervals‡	Fraction of global dataset used in clustering	No. clustering methods	No. MPLDs	Total no. time series
1	All (clustered within time bins independently of depositional setting category)*	1	6	6
1	Marine assemblages	1	4	4
1	Non-marine assemblages	1	4	4
1	Transitional assemblages	1	4	4
1	All (clustered within time bins according to those depositional setting categories)†	1	4	4
2	All (clustered within time bins independently of depositional setting category)*	1	6	6
2	Marine assemblages	1	4	4
2	Non-marine assemblages	1	4	4
2	Transitional assemblages	1	4	4
2	All (clustered within time bins according to those depositional setting categories)†	1	4	4
			Total:	**44**

*clusters in counts may include marine, transitional, and/or non-marine assemblages

† cluster counts equal sums of corresponding marine, transitional, and non-marine counts

‡ Numbers correspond to two sets of chronostratigraphic intervals illustrated in Fig. S6 and outlined in Table S4: (Set 1) 24 chronostratigraphic intervals (mean duration 26.1 Ma ± 18.7) and (Set 2) 19 chronostratigraphic intervals (mean duration 32.1 Ma ± 5.5).

10. Global sedimentary rock outcrop area estimates

The global total, marine, and non-marine sedimentary rock outcrop areas for the time bins and chronostratigraphic intervals in this study were estimated from geologic maps in the Geological Atlas of the World (Choubert and Faure-Muret, 1976) produced by the United Nations Educational, Scientific, and Cultural Organization (UNESCO). The maps occur in 16 sheets, which include all continents at a scale of 1:10,000,000 (1 cm on map=100 km on Earth surface). Sedimentary rocks in the atlas are mapped as continental (i.e. non-marine), flysch (marine), and radiolarite (marine) facies, but most outcrops contain no facies information; for our estimates, we assume the outcrops lacking facies information represent rocks deposited in marine settings. Sedimentary rocks in the atlas are divided among 145 chronostratigraphic classes (corresponding to geological intervals of various thicknesses). Among the 145 chronostratigraphic classes, 123 classes correspond to geologic systems, series, and combinations of systems and/or series of Ediacaran/Phanerozoic-age rocks. The sheets in the atlas were scanned and digitally saved as jpeg files with pixel densities of 400 pixels/inch (157.48 pixels/cm). For each jpeg file, the pixels corresponding to each facies-chronostratigraphic class combination of interest were selected using the magic wand and counted using the histogram window tool in Adobe Photoshop. Then, for each facies-class combination, the cumulative pixel counts among the sheets were determined. These cumulative pixel counts were thereafter divided among 24 chronostratigraphic intervals (mean duration: 26.1 Ma ± 18.7)—the smallest, distinct chronostratigraphic units in the maps—on the basis of the intervals' relative durations in the ICC (Cohen et al., 2013), assuming constant accumulation rates (27 of the 123 chronostratigraphic classes of Ediacaran/Phanerozoic rocks were omitted for these calculations, as they spanned more than six intervals or included quaternary sediments, and therefore, likely do not reflect constant accumulation rates). The 24 chronostratigraphic intervals include three systems (Cambrian–Silurian), 18 series (lower Devonian–Pliocene, excluding Permian series), 2 (lower and upper) Permian intervals, and a Precambrian interval, broadly corresponding to the Ediacaran. For each chronostratigraphic interval and facies, cumulative pixel counts (z) were converted to outcrop areas (*y*, measured in km^2) based on the following conversions (Eqs. S16–S18), which take into account the sheets' digital resolutions and scales:

$$\left(\frac{100\ km}{1\ cm}\right)^2 = \frac{10{,}000\ km^2}{cm^2} \quad \text{(Eq. S16)}$$

$$\left(\frac{157.48\ pixels}{cm}\right)^2 = \frac{24799.95\ pixels^2}{cm^2} \quad \text{(Eq. S17)}$$

$$z\ pixels^2 \times \frac{cm^2}{24799.95\ pixels^2} \times \frac{10{,}000\ km^2}{cm^2} = y\ km^2 \quad \text{(Eq. S18)}$$

These outcrop areas were then divided by their chronostratigraphic intervals' durations in the ICC (Cohen et al., 2013) in order to produce time-normalized rock outcrop area (km^2/Ma) measurements. Lastly, taking into account the relative contributions of the chronostratigraphic intervals to each time bin, these time-normalized rock outcrop area measurements were used to estimate the rock outcrop areas of the time bins used in this study (Dataset S1).

The Atlas includes chronostratigraphic classes for all series in the Devonian-Neogene interval (except for those in the Permian and Carboniferous), which are specified in the ICC (Cohen et al., 2013), so rock outcrop areas were estimated for chronostratigraphic intervals equivalent to all the series in this interval. In contrast, the Atlas does not include chronostratigraphic classes representing Cambrian, Ordovician, or Silurian sub-divisions. Consequently, global sedimentary rock outcrop areas were estimated for chronostratigraphic intervals (Є, O, and S) equivalent to those systems. The Atlas does not explicitly include an Ediacaran (635–541 Ma) chronostratigraphic class, as that system was formally established after publication of the Atlas (Knoll et al., 2006). Nonetheless, the chronostratigraphic class "PP" in the Atlas purportedly begins around ~630 Ma (varying between 600 Ma and 660 Ma among sheets) and ends around the base of the Cambrian (~541 Ma, according to the ICC; Cohen et al., 2013), and includes outcrops of successions that are known to be Ediacaran in age. Hence, the PP class is broadly equivalent to the Ediacaran, and is used herein as the basis for global Ediacaran outcrop area estimation.

Permian outcrops in the Atlas are divided among lower and upper chronostratigraphic classes, which were used to estimate rock outcrop areas for lower (P1) and upper (P2) Permian chronostratigraphic intervals (Dataset S1). It is unclear how these classes and corresponding intervals are related to the three Permian series of the current ICC (Cohen et al., 2013), though historically, the lower Permian includes the Cisuralian series and the upper Permian includes the Guadalupian and Lopingian series (Yugan et al., 1997). Thus, we assume the durations and boundaries of P1 and P2 are equivalent to the Cisuralian and Guadalupian-Lopingian, respectively.

Carboniferous outcrops in the Atlas are divided among lower, middle, and upper chronostratigraphic classes, except in the North American maps, in which they are divided among lower (Mississippian) and upper (Pennsylvanian) classes. Following the current ICC, in which the Carboniferous is sub-divided into Mississippian and Pennsylvanian sub-systems, we estimated the global sedimentary rock outcrop areas for chronostratigraphic intervals C1 and C2 (Dataset S1) equivalent to those two sub-systems, respectively. To estimate the outcrop areas of C1 and C2 in maps of regions outside of North America, we assume that (1) the lower chronostratigraphic class represents the Dinantian geological unit (used in older literature outside of North America), (2) the middle and upper chronostratigraphic classes comprise the Silesian geological unit (used in older literature outside of North America), and (3) approximately 30% of the middle chronostratigraphic class corresponds to Mississippian (C1) outcrop. This approach takes into account stratigraphic work indicating that the Mississippian (C1) corresponds to Dinantian and lowermost Silesian strata and that the Pennsylvanian (C2) corresponds to the Silesian minus its lowermost strata (Heckel and Clayton, 2006).

Although constraints on the absolute ages of boundaries among various series and systems in the Ediacaran-Phanerozoic interval have been refined since the Atlas was published, we can assume such advances in geochronology do not significantly alter the map areas of the chronostratigraphic classes. Historically, the rocks of the various series and systems in the Phanerozoic have been recognized on the basis of stratigraphic criteria (e.g. index fossils), rather than absolute age constraints. Thus, new absolute constraints on the ages of geologic boundaries and local geological units are unlikely to have broadly affected the maps areas.

11. Global sedimentary rock volume estimates

The global marine and non-marine sedimentary rock volumes of the time bins and chronostratigraphic intervals in this study were estimated from published data (Ronov, 1982) on the major lithologic associations, or regularly repeated associations of sedimentary rock, in the Phanerozoic. These data include lithologic association volumes, which were estimated from global maps (1:25,000,000 scale) compiled from various monographs, atlases, and reports on regional geology, stratigraphy, and tectonics. The maps do not visually distinguish between surface and subsurface deposits, although they do include isopachs and deposit thicknesses (Ronov et al., 1977). From these details, for each of 25 exclusive chronostratigraphic classes (generally corresponding to systems and series) of Phanerozoic rocks, volume data were calculated for three non-marine (continental clastic, coal-bearing sand/clay, and glacial clastic) and four marine (sand/clay, carbonate, evaporate, and siliceous) lithologic associations.

To estimate rock volumes for the time bins, we determined the cumulative non-marine (continental clastic+coal-bearing sand/clay+glacial clastic) and marine (marine sand/clay+carbonate+evaporate+siliceous) time-normalized rock volumes (km^3/Ma) for 23 chronostratigraphic intervals (mean duration: 23.4 Ma ± 13.4; Dataset S1). Of the 25 chronostratigraphic classes in the published data, 18 directly equate to chronostratigraphic intervals used in rock outcrop estimation (Dataset S1). The remaining five chronostratigraphic classes—(1) early Carboniferous, (2) middle-late Carboniferous, (3) early Cambrian, (4) middle Cambrian, and (5) late Cambrian—do not directly correspond to such intervals. For our estimation, we assume the early Carboniferous and middle-late Carboniferous classes correspond to the Mississippian (C1) and Pennsylvanian (C2) sub-systems, respectively. In addition, we combine the early, middle, and late Cambrian classes into a single chronostratigraphic interval (Є). (The combining of these intervals likely did not significantly affect the time bin estimates, as they have generally similar rock volumes). Because the published data does not include an Ediacaran or equivalent (e.g. “PP”) chronostratigraphic class, we are left with 23 chronostratigraphic intervals, which span the Phanerozoic (Dataset S1). As in rock outcrop area estimation, the global rock volumes of the chronostratigraphic intervals were divided by their durations (as specified in the ICC; Cohen et al., 2013), yielding time-normalized rock volume (km^3/Ma) measurements, which were then used to estimate the rock volumes of the time bins through consideration of the relative contributions of the chronostratigraphic intervals to each time bin (Dataset S1).

12. North American surface/subsurface rock area estimates

The surface/subsurface areas of North American marine/transitional and non-marine rocks in the times bins in this study were estimated using data (918 stratigraphic columns, 21,239 rock units) accessed from the Macrostrat database of macrostratigraphic packages and lithostratigraphic units (https://macrostrat.org/classic/about.php) on February 4, 2016 (Dataset S1). Estimates of rock area in Macrostrat are based on a Dirichlet tessellation around stratigraphic column control points, as the polygonal areas produced by this tessellation help to account for complex geologic landscapes (e.g. unequal and uneven spread of rock exposure and stratigraphic columns). Estimations of rock area assume that, when a rock unit occurs in one stratigraphic column but not in an adjacent column, the unit extends halfway between the two sections. In this context, for each time bin, rock area was estimated through summing the area of all the polygons containing one or more sedimentary rock units (either on the surface or in the subsurface) belonging to the time bin. Individual polygons can be used in calculations of rock area for multiple time bins (Meyers and Peters, 2011).

13. Description of trends in rock quantities through geologic time

The estimates of the global outcrop areas, global volumes, and North American surface/subsurface areas of the non-marine rocks in the time bins in this study follow similar trends through geologic time (Fig. 10). In general, the quantity (area & volume) of non-marine rock increases from the early-middle Paleozoic to the Pliocene (Quaternary rocks were not included in our estimates). The estimates regarding marine and marine/transitional rocks, on the other hand, follow markedly different patterns through the Phanerozoic. Whereas marine rock outcrop area generally remains constant from the Cambrian to the Cretaceous, the global volume of marine rock and North American surface/subsurface area of the marine/transitional rock fluctuate across several orders of magnitude with maximum volumes/areas recorded in the Ordovician and upper Mesozoic and minimum volumes/areas in the Permian-Triassic interval. These differences reflect the inclusion of subsurface deposits in the estimates of global volumes and North America areas.

14. Statistical testing of cluster counts and proportions

To test for differences among the time bins and time domains, data were compared using Pearson's chi-square (equality and homogeneity) test and Fisher's exact test. The tests were performed in JMP (Sall et al., 2012) and Microsoft Excel. Chi-square equality tests were performed to compare all the time bins in each time series and to assess whether, in terms of cluster count, they are significantly unequal. In these analyses, the observed cluster count of a time bin is its total cluster count (e.g., marine+transitional+non-marine counts, or marine/transitional+non-marine counts), and its expected cluster count is the mean cluster count among the time bins in its time series. Significant ($P < 0.05$) and highly-significant ($P < 0.01$) P values are considered evidence that the time bins are not equal with respect to cluster count. Chi-square tests were also performed on pairs of time domains in their respective time series to assess whether, in terms of their proportions of clusters from various depositional settings, their differences are significant. As some of the chi-square homogeneity tests failed the standard sample size rule (i.e. 80% of the expected counts are >5 and all expected counts >1 in

contingency tables used in calculation of chi-square test statistics), Fisher's exact tests were also performed on pairs of time domains to assess whether differences among their proportions are significant. Significant ($P < 0.05$) and highly-significant ($P < 0.01$) *P* values in these tests are considered evidence that time domains are not homogenous with respect to their proportions.

Randomization tests were performed in Excel to corroborate chi-square equality testing results and to assess if observed trends in cluster count through geologic time could be explained as random variations or sampling artefacts (Huntley et al., 2006). In all randomizations, clusters were randomly shuffled into time bins with equal probabilities of cluster assignment. A total of 40 randomization variants were performed. The differences among these variants include their time bin durations (30.5 or 20.3 my) as well as the clustering methods, MPLDs (either 300 or 1000 km), and data categories (whether assemblages were clustered independently of or according to the marine, transitional, and non-marine depositional setting categories) used in cluster counting. Overall, each randomization variant was repeated 1000 times, and the mean counts, 0.5 percentile values, and 99.5 percentile values of the time bins among the replicates were determined and compared to the observed cluster counts. For each randomization variant, if any of the observed cluster counts fell outside of the 99% CI envelope, then the observed trend could not be explained by random variations. Conversely, if all observed values fell inside the 99% CI, then the trend could be explainable as a sampling artefact.

Linear polynomial regression models were fit to the time bins' proportions of clusters (y) and ages (x) in order to assess whether the proportions of clusters from marine, transitional, marine/transitional, and non-marine depositional settings significantly change through time. Linear and non-linear relationships between proportion and time were modelled with 1^{st}-degree and higher-degree polynomials, respectively. To assess the fits of the models, *P* values were tabulated through analysis of variance (ANOVA) *F*-testing. Significant ($P < 0.05$) and highly-significant ($P < 0.01$) *F*-test *P* values are considered evidence that the regression models fit time series better than data means. The fit of any regression model to the data (except for linear model with slope = 0) represents significant evidence that the proportion of clusters changes through time. To assess the accuracy of the *F*-tests, which assume that residuals are normally-distributed, Shapiro-Wilk and Jarque-Bera tests were performed on the residuals in the regression analyses; *P* values less than 0.05 and 0.01 denote statistically significant and highly significant departures of residuals from normality (i.e. *F*-test may have low statistical power).

The time bins' cluster counts were plotted against their corresponding rock areas, rock volumes, and sea levels to assess for potential correlations among these variables. Analyses involving non-marine cluster counts did not include time bins older than 430 Ma, which pre-date the earliest robust fossil evidence of widespread terrestrial plant (Kenrick and Crane, 1997) and animal (Shear and Selden, 2001) life. In addition, analyses involving global rock volume and sea level did not include time bins older than 531.7 Ma and Ma 552 Ma, respectively, due to data limitations. The results of these analyses—which were repeated for time series based on various clustering methods, time bin durations, MPLDs, and data categories used in cluster counting—are presented as *F*-test *P*, R, and coefficient of determination (R^2) values. Significant ($P < 0.05$) and highly-significant ($P < 0.01$) *F*-test *P* values are considered evidence of correlations. To verify that the statistically significant results of this work are robust to autocorrelation, the analyses were repeated with data subjected to first differencing (see Supplementary Information).

15. First difference analyses

To verify the statistically significant results in correlation analyses of the time series variables (e.g., cluster counts and rock quantities of equal duration time bins), first differenced cluster counts were correlated against first differenced global rock outcrop area, global rock volume, and North American surface/subsurface area data. Results are presented as F-test P, R, and R^2 values (Fig. S7). Significant ($P < 0.05$) and highly-significant ($P < 0.01$) P values indicate correlations that are robust to non-constant mean, variance, and autocorrelation within time series. Overall, these analyses corroborate the results that suggest non-marine cluster count is positively correlated with non-marine rock quantity. Correlations between non-marine cluster count and global non-marine rock outcrop area and between non-marine cluster count and global non-marine rock volume are supported by F-test P values < 0.05 for 30.5 my duration time bins and MPLDs 500–1000 km (Fig. S7). Analyses of 20.33 my duration time bins involving these variables did not yield significant results (Fig. S7), but this is likely because the rock outcrop areas and volumes were estimated from chronostratigraphic intervals, which in general, are greater in duration than the 20.33 my time bins. Differences among contiguous 20.33 time bins, therefore, may be more averaged than in 30.5 my duration time bins. Likewise, correlations analyses comparing North American non-marine cluster count and North American surface/subsurface rock area first differences did not yield statistically significant results, which may reflect small samples sizes from North America (the majority of time bins have North American non-marine cluster counts <1 at all MPLDs). Nonetheless, the results corroborate the correlation analyses (Fig. 11) indicating non-marine cluster count is positively correlated with non-marine rock quantity.

First difference analyses do not provide compelling evidence for a correlation between marine/transitional cluster count and marine rock quantity, regardless of MPLD or time bin duration (Fig. S7). Correlations between North American marine/transitional cluster count and North American marine/transitional surface/subsurface rock area supported by F-test $P < 0.05$ (30.5 my duration time bins and most MPLDs ≤ 1000 km) provide some evidence for a relationship between the variables, but these results are not supported by correlation analyses comparing marine/transitional cluster count to global marine rock outcrop area or volume.

16. Results of clustering assemblages with chronostratigraphic intervals

Assigning data points to time bins, which do not exactly match geologic units, can introduce errors into datasets. Points with age uncertainties may be assigned to bins that do not accurately reflect their actual ages. If so, the values calculated for time bins (e.g. means) will deviate from their true values. In the context of this contribution, in which we have assigned fossil assemblages to time bins based on their mean ages (mean uncertainty: 5 Ma ± 5), the bin assignments of assemblages with chronostratigraphically constrained age ranges spanning multiple bins may not accurately reflect their true ages, and the counts and proportions of some time bins may be erroneous. Such errors could affect the results, particularly if the errors are non-random and disproportionately affect the time bins. To confirm that errors related to

assigning assemblages to equal duration time bins did not significantly affect the results, we hierarchically clustered assemblages within geologically defined chronostratigraphic intervals (Dataset S1) using the complete-linkage method and calculated counts and proportions of marine, transitional, and non-marine clusters for various MPLDs. From this data, we produced cluster count and proportion time series (Table S3, Fig. S6) for comparison with the main results (Figs. 7, 12, 14, S9-S11). In addition, we conducted correlation analyses—comparing cluster counts to global sedimentary rock outcrop areas and volumes—to corroborate the results of the analyses involving equal duration time bins. Notably, as this work made use of chronostratigraphic intervals corresponding to the chronostratigraphic intervals used in estimating rock outcrop areas and volume, the derivation of these variables for the intervals did not require any intricate conversions beyond simple arithmetic. These correlation analyses, therefore, also broadly test whether rock outcrop area and volume conversions between chronostratigraphic classes and equal duration time bins affected the outcomes of the main work.

Overall, we used chronostratigraphic intervals to generate time series of two types (Fig. S6). Each time series of the first type (time series type 1 in Table S4, Fig. S6a, b) includes 24 chronostratigraphic intervals representing geologic systems and series, excluding a single interval (P2 in Table S4), which represents a combined Guadalupian and Lopingian interval. The intervals in this series vary considerably in duration (mean duration 26.1 Ma ± 18.7), but each one corresponds directly to a chronostratigraphic interval used in estimating rock outcrop area and volume. Each time series of the second type (time series type 2 in Table S4, Fig. S6c, d) includes 19 chronostratigraphic intervals representing geologic systems, series, and combinations of series and/or Ediacara-type fossil biozones. All intervals younger than the Cambrian correspond to chronostratigraphic intervals or combinations of those intervals used in estimating rock outcrop areas and volume. These intervals notably exhibit less variation in duration (mean duration 32.1 Ma ± 5.5), meaning that in terms of the time represented by each cluster, the clusters are relatively more equivalent to each other than those in time series of the first type. As such, these intervals were used for correlation analysis (Fig. S8a, b), as biases created by the unequal durations of the intervals are relatively minor. The intervals' cluster counts were plotted against their corresponding rock outcrop areas and volumes (correlations with sea level did not produce significant results). Analyses involving non-marine cluster counts did not include intervals older than the lower Devonian, which pre-date the earliest robust fossil evidence of widespread terrestrial plant (Kenrick and Crane, 1997) and animal life (Shear and Selden, 2001). In addition, analyses involving global rock volume did not include intervals older than the Cambrian due to data limitations. The results of these analyses—which were repeated for time series based on various MPLDs used in cluster counting—are presented as *F*-test *P*, R, and R^2 values. Significant ($P < 0.05$) *F*-test *P* values are considered evidence of correlations. To verify that the statistically significant results of this work are robust to autocorrelation, the analyses were repeated with data subjected to first differencing (Fig. S8c, d).

Not surprisingly, cluster count time series of the first type (Fig. S6b) differ from all other time series, having markedly low cluster counts in Cenozoic intervals (N2, N2, Pg3, Pg2, and Pg1). This result is likely a consequence of the short geologic durations of these intervals, as compared to all others in these time series. Indeed, the shortest intervals in these time series generally have the lowest cluster counts, and vice versa. Taking this relationship into

consideration, the clusters in the time series of the first type do not represent equivalent units at any MPLD, and their counts do not capture unambiguous patterns in the fossil record.

Time series of the second type, in which chronostratigraphic intervals represent broadly equivalent geologic time spans (mean duration 32.1 Ma ± 5.5), generally corroborate the findings from analyses involving time bins of equal durations. According to the results, the dataset includes over-abundances of assemblages in the Ediacaran (White Sea and Avalon stages) and lower Cretaceous relative to geographic expansiveness (Fig. S6c versus d). When geospatial clustering is taken into consideration, clusters increase in number (geospatial spread) from the lower Ediacaran into the Phanerozoic, peak in the Cambrian, and decline through the lower-middle Paleozoic before rising through the remainder of the Phanerozoic, excluding intervals in the late Triassic and latest Cretaceous, which include relatively few clusters of assemblages.

Cluster proportion time series further corroborate the results of the main analyses involving equal duration time bins. Regardless of the chronostratigraphic intervals used, the results indicate that exceptional preservational conditions shifted from predominantly marine depositional settings in the Ediacaran-early Paleozoic to transitional and non-marine settings in the Silurian-Carboniferous and Permian-Neogene intervals, respectively (Figs. S6e–g). In addition, the data indicates that exceptional preservation rose in frequency within marine and transitional settings in the Jurassic and late Cretaceous.

The supplementary correlation analyses (Fig. S8a, b) provide additional support for the main results. The positive correlation between non-marine cluster count and non-marine rock outcrop area is statistically significant at all MPLDs with high R^2 values (>0.70) for clustered assemblages (MPLDs equal to 200 km, 600 km, and 1000 km in Fig. S8a). First-difference testing (Fig. S8c) confirms that the correlation is robust, so long as the data has been standardized via clustering. Likewise, the correlation between non-marine cluster count and rock volume is statistically significant at all MPLDs with similarly high R^2 values (>0.60) for clustered assemblages (MPLDs equal to 200 km, 600 km, and 1000 km in Fig. S8b). Again, first-difference testing (Fig. S8d) generally confirms that the correlation is robust, so long as the data has been standardized via clustering. The analyses yield no significant evidence of correlation between marine cluster count and rock outcrop area (Fig. S8a), and although some analyses provide evidence for a correlation between marine cluster count and rock volume (Fig. S8b, d), marine rock volume accounts for only a fraction of the variation in marine cluster count (R^2 values no more than 0.41). Thus, the analyses involving cluster counts and proportions—derived via hierarchical clustering of assemblages within geologically defined chronostratigraphic intervals with direct estimates of global rock outcrop area and volume—confirm that errors caused by assigning assemblages to equal duration time bins did not affect the outcomes of the overall work.

Table S4. Chronostratigraphic intervals used in hierarchical clustering work (Fig. S6, S8).

Time series type[1]	Interval	Chronostratigraphic units included within interval	Lower age (Ma)	Upper age (Ma)	Duration (Ma)
1	N2	Pliocene	2.58	5.33	2.75
1	N1	Miocene	5.33	23.03	17.70
1	Pg3	Oligocene	23.03	33.90	10.87
1	Pg2	Eocene	33.90	56.00	22.10
1	Pg1	Paleocene	56.00	66.00	10.00
1 and 2	K2	Upper Cretaceous	66.00	100.50	34.50
1 and 2	K1	Lower Cretaceous	100.50	145.00	44.50
1	J3	Upper Jurassic	145.00	163.50	18.50
1	J2	Middle Jurassic	163.50	174.10	10.60
1 and 2	J1	Lower Jurassic	174.10	201.30	27.20
1 and 2	T3	Upper Triassic	201.30	237.00	35.70
1	T2	Middle Triassic	237.00	247.20	10.20
1	T1	Lower Triassic	247.20	252.17	4.97
1	P2[2]	Lopingian and Guadalupian	252.17	272.30	20.13
1 and 2	P1	Cisuralian	272.30	298.90	26.60
1 and 2	C2	Pennsylvanian	298.90	323.20	24.30
1 and 2	C1	Mississippian	323.20	358.90	35.70
1	D3	Upper Devonian	358.90	382.70	23.80
1	D2	Middle Devonian	382.70	393.30	10.60
1 and 2	D1	Lower Devonian	393.30	419.20	25.90
1 and 2	S	Silurian	419.20	443.40	24.20
1 and 2	O	Ordovician	443.40	485.40	42.00
1	Є	Cambrian	485.40	541.00	55.60
1	E[3]	Ediacaran	541.00	630.00	89.00
2	N2+N1+Pg3	Pliocene, Miocene, and Oligocene	2.58	33.9	31.32
2	Pg2+Pg1	Eocene and Paleocene	33.9	66	32.1
2	J3+J2	Upper and Middle Jurassic	145	174.1	29.1
2	T2+T1+P2	Middle Triassic, Lower Triassic, Lopingian, and Guadalupian	237	272.3	35.3
2	D3+D2	Upper and Middle Devonian	358.9	393.7	34.8
2	Є3+Є2[4]	Cambrian (minus Terreneuvian)	485.4	521	35.6
2	Є1+E4[5]	Terreneuvian and Nama "stage"	521	551	30
2	E3+E2[6]	White Sea and Avalon "stages"	551	580	29
2	E1[6]	Marinoan-Gaskiers "stage"	580	613	33

[1] Numbers correspond to the different time series types, which were generated using different intervals and illustrated in Fig. S6: (1) 24 chronostratigraphic intervals (mean duration 26.1 Ma ± 18.7) and (2) 19 chronostratigraphic intervals (mean duration 32.1 Ma ± 5.5).

[2] This interval broadly matches the P2 chronostratigraphic interval used in compiling rock quantity data.

[3] The Ediacaran is broadly equivalent to the "PP" chronostratigraphic interval used in estimating rock outcrop area.

[4] We have divided the Cambrian into lower, middle, and upper units, and assume they have roughly equal rock outcrop areas and volumes, as suggested by available volume data (Ronov, 1982).

[5] The rock volume estimate for this bin reflects only the Cambrian. We assume the contributions of the terminal Ediacaran to the volume of this bin is negligible (Dataset S1). For rock outcrop area, we use an overtly high estimate, assuming that this bin includes a third of all Cambrian outcrop area and virtually all Ediacaran outcrop.

[6] No global rock volumes are available for these intervals. For rock outcrop area, we have divided the "PP" estimate from the Geologic Atlas of the World among the two intervals, assuming that they have equal areas.

17. References for supplementary information

Bertrand-Sarfati, J., Moussine-Pouchkine, A., Amard, B., Ait Kaci Ahmed, A., 1995. First Ediacaran fauna found in western Africa and evidence for an Early Cambrian glaciation. Geology 23, 133–136.

Choubert, G., Faure-Muret, A., 1976. Geological atlas of the world. 1:10,000,000. 22 sheets with explanations. UNESCO, Paris, France.

Cohen, K.M., Finney, S.C., Gibbard, P.L., Fan, J.-X., 2013. The ICS International Chronostratigraphic Chart. Episodes 36, 199–204.

Dornbos, S.Q., Oji, T., Kanayama, A., Gonchigdorj, S., 2016. A new Burgess Shale-type deposit from the Ediacaran of western Mongolia. Scientific Reports 6, 1–5.

Hartigan, J.A., 1981. Consistency of Single Linkage for High-Density Clusters. Journal of the American Statistical Association 76, 388–394.

Heckel, P.H., Clayton, G., 2006. The Carboniferous System. Use of the new official names for the subsystems, series, and stages. Geologica Acta 4, 403–407.

Hoffman, P.F., Li, Z.-X., 2009. A palaeogeographic context for Neoproterozoic glaciation. Palaeogeography Palaeoclimatology Palaeoecology 277, 158–172.

Huntley, J.W., Xiao, S., Kowalewski, M., 2006. On the morphological history of Proterozoic and Cambrian acritarchs, In: Xiao, S., Kaufman, A.J. (Eds.), Neoproterozoic Geobiology and Paleobiology. Springer, Dordrecht, the Netherlands, pp. 23–56.

Kenrick, P., Crane, P.R., 1997. The origin and early evolution of plants on land. Nature 389, 33–39.

Knoll, A.H., Walter, M.R., Narbonne, G.M., Christie-Blick, N., 2006. The Ediacaran Period: a new addition to the geologic time scale. Lethaia 39, 13-30.

Meyers, S.R., Peters, S.E., 2011. A 56 million year rhythm in North American sedimentation during the Phanerozoic. Earth and Planetary Science Letters 303, 174–180.

Milligan, G., 1980. An examination of the effect of six types of error perturbation on fifteen clustering algorithms. Psychometrika 45, 325–342.

Milligan, G.W., Cooper, M.C., 1987. Methodology review: Clustering methods. Applied Psychological Measurement 11, 329–354.

Murtagh, F., Contreras, P., 2012. Algorithms for hierarchical clustering: an overview. Wiley Interdisciplinary Reviews: Data Mining and Knowledge Discovery 2, 86–97.

Muscente, A.D., Hawkins, A.D., Xiao, S., 2015. Fossil preservation through phosphatization and silicification in the Ediacaran Doushantuo Formation (South China): A comparative synthesis. Palaeogeography, Palaeoclimatology, Palaeoecology 434, 46–62.

Narbonne, G.M., Xiao, S., Gehling, J.G., Shields-Zhou, G.A., 2012. The Ediacaran Period, In: Gradstein, F.M., Ogg, J.G., Schmitz, M., Ogg, G. (Eds.), Geological Time Scale 2012. Elsevier, Oxford, pp. 413–435.

Qin, X., Müller, R.D., Cannon, J., Landgrebe, T.C.W., Heine, C., Watson, R.J., Turner, M., 2012. The GPlates geological information model and markup language. Geoscientific Instrumentation, Methods and Data Systems 1, 111–134.

Ronov, A.B., 1982. The Earth's sedimentary shell (quantitative patterns of its structures, compositions, and evolution): The 20th V.I. Vernadskly lecture, March 12, 1978. International Geology Review 24, 1365–1388.

Ronov, A.B., Seslavinskiy, K.B., Khain, V.Y., 1977. Cambrian lithologic associations of the world. International Geology Review 19, 373–394.

Rosenberg, M.S., Anderson, C.D., 2011. PASSaGE: Pattern Analysis, Spatial Statistics and Geographic Exegesis. Version 2. Methods in Ecology and Evolution 2, 229-232.

Sall, J., Lehman, A., Stephens, M.L., Creighton, L., 2012. JMP Start Statistics: A Guide to Statistics and Data Analysis Using JMP, Fifth Edition. SAS Institute.

Shear, W.A., Selden, P.A., 2001. Rustling in the undergrowth: Animals in early terrestrial ecosystems, In: Gensel, P.G., Edwards, D. (Eds.), Plants Invade the Land: Evolutionary and Environmental Perspectives. Columbia Uniersity Press, New York, pp. 29–51.

Sokal, R., Milchener, C., 1958. A statistical method for evaluating systematic relationships. University of Kansas Science Bulletin 38, 1409–1438.

Williams, S.E., Müller, R.D., Landgrebe, T.C.W., Whittaker, J.M., 2012. An open-source software environment for visualizing and refining plate tectonic reconstructions using high-resolution geological and geophysical data sets. GSA Today 22, 4–9.

Wright, N., Zahirovic, S., Müller, R.D., Seton, M., 2013. Towards community-driven paleogeographic reconstructions: Integrating open-access paleogeographic and paleobiology data with plate tectonics. Biogeosciences 10, 1529–1541.

Yuan, X., Chen, Z., Xiao, S., Zhou, C., Hua, H., 2011. An early Ediacaran assemblage of macroscopic and morphologically differentiated eukaryotes. Nature 470, 390–393.

Yugan, J., Wardlaw, B.R., Glenister, B.F., Kotlyar, G.V., 1997. Permian chronostratigraphic subdivisions. Episodes 20, 10–15.